arXiv:2008.03840v1 [cond-mat.soft] 9 Aug 2020

Theory of electrolytes including steric, attractive, and hydration interactions

Ryuichi Okamoto[a],* Kenichiro Koga[a,b], and Akira Onuki[c]
[a] Research Institute for Interdisciplinary Science, Okayama University, Okayama 700-8530, Japan
[b] Department of Chemistry, Faculty of Science, Okayama University, Okayama 700-8530, Japan
[c] Department of Physics, Kyoto University, Kyoto 606-8502, Japan
(Dated: February 1, 2022)

We present a continuum theory of electrolytes composed of a waterlike solvent and univalent ions. First, we start with a density functional $\mathcal{F}$ for the coarse-grained solvent, cation, and anion densities, including the Debye-Hückel free energy, the Coulombic interaction, and the direct interactions among these three components. These densities fluctuate obeying the distribution $\propto \exp(-\mathcal{F}/k_BT)$. Eliminating the solvent density deviation in $\mathcal{F}$, we obtain the effective non-Coulombic interactions among the ions, which consist of the direct ones and the solvent-mediated ones. We then derive general expressions for the ion correlation, the apparent partial volume, and the activity and osmotic coefficients up to linear order in the average salt density $n_{\rm s}$. Secondly, we perform numerical analysis using the Mansoori-Carnahan-Starling-Leland model [J. Chem. Phys. **54**, 1523 (1971)] for three-component hardspheres. The effective interactions sensitively depend on the cation and anion sizes due to competition between the steric and hydration effects, which are repulsive between small-large ion pairs and attractive between symmetric pairs. These agree with previous experiments and Collins' rule [Biophys. J. **72**, 65 (1997)]. We also give simple approximate expressions for the ionic interaction coefficients valid for any ion sizes.

I. INTRODUCTION

The nature of how ions interact among themselves and with water has been studied extensively in physical chemistry[1,2]. In their seminal work in 1923, Debye and Hückel[3] (DH) calculated the free energy correction due to the long-range ion-ion correlation[1,4]. To leading-order in the average salt density $n_{\rm s}$, it is of order $n_{\rm s}^{3/2}$ and is determined by the solvent dielectric constant ϵ and the ion valences, so it is exceptionally *ion-nonspecific*. On the other hand, diverse phenomena sensitively depend on the ion species in liquid water and aqueous mixtures[5–7], where the short-range ion-ion and ion-solvent interactions come into play. Such *ion-specificity* was originally reported by Hofmeister[8] 130 years ago in the salting-out/salting-in effect of proteins. The extended DH theory[1–4,9] and the Born theory of hydration[10–12] already assumed certain ionic radii specifically depending on the ion species.

Since the early period of research[1,2,13–19], there have been a great number of measurements of the mean activity and osmotic coefficients, $\gamma_\pm$ and φ. They have been expanded as $1 + A\sqrt{n_{\rm s}} + Bn_{\rm s} + \cdots$ for small $n_{\rm s}$, where the second term represents the DH part with an ion-nonspecific coefficient A. However, the third term depends on the short-range interactions. and the coefficient B has been determined empirically for each ion pair. On the other hand, the apparent partial volume of salts[11,12,20–23], written as $v_{\rm s}^{\rm ap}$, exhibits unique ion-size-dependence different from those of $\gamma_\pm$ and φ.

In early *primitive* theories[4,24–30], the ions are hardspheres with charges $\pm q$, while the solvent is treated as a uniform continuum without any degrees of freedom (which much simplifies the calculations). Some simulations treated cations and anions without solvent particles to confirm these theories[31,32]. We also mention general statistical mechanical studies[33–37] and molecular dynamics (MD) simulations[38–46], which attempted to take into account the solvent effects in various manners. Some simulations[38,43,44,46] aimed to determine the force-field parameters in simulation for each ion pair using the Kirkwood-Buff (KB) integrals[47]. From our viewpoint, it is still difficult to catch the overall physical picture of the observed ion-specificity from these papers.

As a key to the problem, Widom *et al.*[48–50] calculated the second osmotic virial coefficient $B_2 = -G_{22}^0/2$ for a nonionic solute in a one-component solvent[51], where G_{22}^0 is the dilute limit of the solute-solute KB integral. Including the solvent degrees of freedom, they found

$$B_2 = B_2'' - (v_2^0 - k_BT\kappa_{\rm w})^2/2k_BT\kappa_{\rm w}, \tag{1}$$

where B_2'' arises from the direct solute-solute interaction at a fixed solvent density. The second volume term is due to the solvent-mediated interaction, where v_2^0 is the solute partial volume and $\kappa_{\rm w}$ is the solvent isothermal compressibility. It is largely negative for nearly incompressible solvents with small $\kappa_{\rm w}$, leading to solute-solute attraction (particularly for large v_2^0). For electrolytes, the corresponding contributions have been missing in the previous theories[24–31]. In this paper, we extend Eq.(1) to dilute electrolytes.

On electrolytes, there have been numerous continuum theories based on the Poisson-Boltzmann equation in various situations[52–56]. To account for the excluded volumes, the space-filling relation $\sum_i v_i n_i = 1$ has been widely assumed[57–60], where v_i is a molecular volume of the i-th component with density n_i. Furthermore, convenient is a continuum model of hardsphere mixtures by Mansoori, Carnahan, Starling, and Leland (MCSL)[61], as

* okamoto-ryuichi@okayama-u.ac.jp

used in subsequent papers[54,62,63]. It is a generalization of the Carnahan and Starling model of monodisperse hardspheres[64]. Using the MCSL model for neutral fluids, we studied small bubbles in water due to dissolved gases[65,66] and phase behavior in ternary mixtures[67] such as water-alcohol-hydrophobic solute[68]. In the latter, the second term in Eq.(1) and another contribution from the concentration fluctuations were crucial.

In this paper, we first present a statistical-mechanical theory setting up a free energy functional for the densities n_1, n_2, and n_3 of the solvent, the cations, and the anions, respectively. Expressing the deviation $\delta n_1 = n_1 - \langle n_1 \rangle$ in terms of n_2 and n_3, we obtain the effective ion-ion interaction coefficients, written as $U_{ij}^{\rm eff}$ $(i, j = 2, 3)$, which have bilinear volume terms as B_2 in Eq.(1). Using the continuum MCSL and Born models, we show that $U_{ij}^{\rm eff}$ tend to be negative (attractive) for symmetric ion pairs, but tend to be positive (repulsive) for small-large pairs. These agree with experiments and Collins' empirical rule[69–71]. Mathematically, the total packing fraction arises mainly from the solvent particles in our theory but from the ions only in the primitive theories[4,24–30]. This leads to largely different results in the two approaches.

Small-large ion pairs exhibit unique behavior in water, which include NaI as a relatively mild example and $NaBPh_4$ as an extreme one. In the latter, tetraphenylborate BPh_4^- consists of four phenyl rings bonded to an ionized boron[72–74]. In aqueous mixtures, adding a small amount of $NaBPh_4$ is known to produce mesophases due to preferential solvation[53,75–78].

The organization of this paper is as follows. In Sec.II, we will start with a free energy functional including the DH free energy. We will then study the thermal density fluctuations accounting for the solvent-mediated correlations. In Sec.III, we will study the thermodynamics of electrolytes. In Sec.IV, we will first examine the ion volume and the ion-ion interaction and then present numerical analysis of various physical quantities.

II. FLUCTUATIONS IN ELECTROLYTES

In our theory, the solvent is a nearly incompressible, one-component liquid, which is also called water, and the ions have the unit charges $\pm e$. The salt or base added is assumed to dissociate completely. We do not treat Bjerrum dipoles[1,28,29,79–87] as an independent entity (see Appendix A). The effective ionic diameters are not much lager than that of the solvent $d_1 (\cong 3$Å for water). We study the bulk properties without applied electric field. Thus, under the periodic boundary condition, the electrolyte is in a large $L \times L \times L$ box with volume $V = L^3$. Generalization to the case of multivalent ions is straightforward[4] (see below Eq.(37)). In this paper, the temperature T is fixed and its dependence of the physical quantities is not written explicitly.

A. Free energy functional $\mathcal{F}$ of electrolytes

We write the coarse-grained number densities of water, cations, and anions as n_1, n_2, and n_3, respectively. Their Fourier components $n_i(\boldsymbol{q}) = \int d\boldsymbol{r} n_i(\boldsymbol{r}) \exp(-i\boldsymbol{q}\cdot\boldsymbol{r})$ have wave numbers smaller than an upper cut-off Λ. In this section, assuming that Λ is smaller than the Debye wave number κ, we examine the thermal fluctuations of $n_i(\boldsymbol{q})$ with $q < \Lambda$. They obey the distribution $\propto \exp[-\mathcal{F}/k_BT]$, where we introduce the free energy functional,

$$\mathcal{F}(\Lambda) = \int d\boldsymbol{r} f + \frac{1}{2}\int d\boldsymbol{r}\rho\Phi. \tag{2}$$

Here, f depends on n_1, n_2, and n_3 in the local density approximation. The second term represents the long-range Colombic intercation, where $\rho = e(n_1 - n_2)$ is the charge density and Φ is the electric potential related by $-\nabla\cdot\epsilon\nabla\Phi = 4\pi\rho$, where ϵ is the dielectric constant.

We expand f up to the second order in n_2 and n_3 as

$$f = f_{\rm w}(n_1) + k_BT\sum_{i=2,3}[\ln(n_i\lambda_i^3) - 1 + \nu_i(n_1)]n_i \\ -\frac{1}{12\pi}k_BT\kappa^3 + \frac{1}{2}\sum_{i,j=2,3}U_{ij}(n_1)n_in_j. \tag{3}$$

The first term $f_{\rm w}(n_1)$ is the free energy density of pure solvent. In the second term, λ_i is the thermal de Broglie length and $k_BT\nu_i(n_1)$ is the solvation chemical potential per ion due to the interactions between an isolated ion of species i and the solvent. The third term is the DH free energy density in the limit of low ion densities[1,3,4,9], where κ is the the Debye wave number,

$$\kappa = [4\pi e^2(n_2 + n_3)/\epsilon(n_1)k_BT]^{1/2}. \tag{4}$$

In the last term, $U_{ij}(n_1)$ represents the short-range direct interactions between ion species i and j under influence of the solvent. Here, $\epsilon(n_1)$, $\nu_i(n_1)$, and $U_{ij}(n_1)$ strongly depend on n_1 in liquids.

The DH free energy can be calculated from the average of an excess electric field around each ion, which is produced by the other ions with separation distances shorter than κ^{-1}. Thus, to use the DH theory, we need to assume $\Lambda < \kappa$. Debye and Hückel also introduced a closest distance around each ion in the ion-ion correlation[1–4,9], which is written as a_2 for the cations and as a_3 for the anions. The DH free energy density is thus given by[88]

$$f_{\rm DH} = -\frac{1}{3}k_BT\ell_B\kappa\sum_{i=2,3}n_i\tau(a_i\kappa) \\ = -\frac{1}{12\pi}k_BT\kappa^3 + \frac{1}{2}\sum_{i,j=2,3}u_{ij}^{\rm ex}n_in_j + \cdots, \tag{5}$$

where $\tau(x) = 3[\ln(1+x) - x + x^2/2]/x^3$ and and $\ell_B = e^2/\epsilon(n_1)k_BT$ is the Bjerrum length (= 7 Å in ambient water). In the second line, using $\tau(x) = 1 - 3x/4 + \cdots$ for $x \ll 1$, we write the first correction for $a_i\kappa \ll 1$ with

$$u_{ij}^{\rm ex} = \pi k_BT\ell_B^2(a_i + a_j). \tag{6}$$

Here, $u_{ij}^{\rm ex} = 34 k_B T d_1^3$ for $a_2 = a_3 = d_1 = 3$ Å in ambient water. We assume that $u_{ij}^{\rm ex}$ are included in U_{ij} in Eq.(3). In Sec.IV, we will calculate the excess parts $U_{ij} - u_{ij}^{\rm ex}$.

We suppose an equilibrium reference state, where the average water and salt densities are written as

$$\langle n_1 \rangle = n_{\rm w}, \quad \langle n_2 \rangle = \langle n_3 \rangle = n_{\rm s}. \tag{7}$$

Under the overall charge neutrality, we use the mean solvation and interaction coefficients,

$$\nu = (\nu_2 + \nu_3)/2, \tag{8}$$
$$U = (U_{22} + U_{33})/2 + U_{23}. \tag{9}$$

We also introduce the incompressibility parameter,

$$\epsilon_{\rm in} = n_{\rm w} k_B T \kappa_{\rm w}, \tag{10}$$

where $\kappa_{\rm w} = 1/(n_{\rm w}^2 \partial^2 f_{\rm w}/\partial n_{\rm w}^2)$ is the solvent isothermal compressibility. Here, $\epsilon_{\rm in} \ll 1$ for nearly incompressible liquids. For ambient liquid water ($T = 300$ K and $p = 1$ atm), we have $\kappa_{\rm w} \cong 4.5 \times 10^{-4}$/MPa and $\epsilon_{\rm in} \cong 0.062$.

B. Thermal fluctuations and ion volumes

We here examine the long-wavelength density fluctuations to derive ion volumes. To this end, we superimpose small density deviations $\delta n_i(\boldsymbol{r})$ on the averages as

$$n_1 = n_{\rm w} + \delta n_1, \quad n_i = n_{\rm s} + \delta n_i \ (i = 2, 3). \tag{11}$$

where δn_i have Fourier components $n_i(\boldsymbol{q})$ with $q < \Lambda$.

The deviation $\delta\mathcal{F} = \mathcal{F} - F$ of the free energy functional starts from second-order terms as[67]

$$\delta\mathcal{F} = \frac{1}{2} \int_{\boldsymbol{q}} \Big[\sum_{i,j=1,2,3} f_{ij} n_i(\boldsymbol{q}) n_j(\boldsymbol{q})^* + \frac{4\pi}{\epsilon q^2} |\rho_{\boldsymbol{q}}|^2 \Big], \tag{12}$$

where $\int_{\boldsymbol{q}} = V^{-1} \sum_{\boldsymbol{q}}$ represents the summation over the wave vector $\boldsymbol{q}$. The second derivatives of f with respect to the densities at fixed T are written as

$$f_{ij} = \partial^2 f / \partial n_i \partial n_j, \tag{13}$$

which are the values at $n_1 = n_{\rm w}$ and $n_2 = n_3 = n_{\rm s}$. In Eq.(12), the Coulombic term arises from the second term in Eq.(2) with $\rho_{\boldsymbol{q}} = e[n_2(\boldsymbol{q}) - n_3(\boldsymbol{q})]$. Then, Eq.(3) gives

$$f_{11} = 1/(n_{\rm w}^2 \kappa_{\rm w}) + 2 k_B T \nu'' n_{\rm s}, \tag{14}$$
$$f_{1i} = k_B T [\nu_i' + (3\epsilon'/4\epsilon) \ell_B \kappa] + (U_{i2}' + U_{i3}') n_{\rm s}, \tag{15}$$
$$f_{ij} = k_B T (\delta_{ij} - \ell_B \kappa/8)/n_{\rm s} + U_{ij}, \tag{16}$$

where $i, j = 2, 3$. Here, $\nu_i' = \partial \nu_i / \partial n_1$, $\nu'' = \partial^2 \nu / \partial n_1^2$, $\epsilon' = \partial \epsilon / \partial n_1$, and $U_{ij}' = \partial U_{ij}/\partial n_1$ at $n_1 = n_{\rm w}$ (see the value of ν'' for NaCl below Eq.(45)). Data of ϵ for ambient water indicate[89,90]

$$n_{\rm w} \epsilon'/\epsilon = \kappa_{\rm w}^{-1} (\partial \ln \epsilon / \partial p)_T = 1.1. \tag{17}$$

In the brackets in Eq.(12), the solvent-ion coupling arises from $[f_{12} n_2(\boldsymbol{q}) + f_{13} n_3(\boldsymbol{q})] n_1(\boldsymbol{q})^*$. Thus, we introduce the deviation of the particle volume fraction[67],

$$\begin{aligned} \delta\phi_v &= [\delta n_1 + (f_{12}/f_{11}) \delta n_2 + (f_{13}/f_{11}) \delta n_3]/n_{\rm w} \\ &\cong n_{\rm w}^{-1} \delta n_1 + v_2^* \delta n_2 + v_3^* \delta n_3. \end{aligned} \tag{18}$$

The first line of Eq.(18) can be used for general $n_{\rm s}$. In the second line v_i^* are ion volumes at infinite dilution,

$$v_i^* = \lim_{n_{\rm s} \to 0} f_{1i}/f_{11} n_{\rm w} = \epsilon_{\rm in} \nu_i' \quad (i = 2, 3). \tag{19}$$

For nonionic mixtures, v_i^* corresponds to $v_2^0 - k_B T \kappa_{\rm w}$ in Eq.(1)[48–50] and to $v_3^{\rm in}$ in our recent paper[67]. See also Eq.(21) and the subsequent sentences.

We can then rewrite $\delta\mathcal{F}$ in Eq.(12) as

$$\delta\mathcal{F} = \frac{1}{2} n_{\rm w}^2 f_{11} \int d\boldsymbol{r} |\delta\phi_v|^2 + \delta\mathcal{F}_{\rm ion}. \tag{20}$$

where $n_{\rm w}^2 f_{11} \cong \kappa_{\rm w}^{-1}$. Here, the first term represents the *steric interaction*, which suppresses the thermal fluctuations of $\delta\phi_v$ for small $\kappa_{\rm w}$. Namely, δn_1 tends to decrease by $n_{\rm w}(v_2^* \delta n_2 + v_3^* \delta n_3)$ on the average at long wavelengths. This interaction can be derived for any multi-component fluids[60], where $\delta\phi_v \to 0$ as $\kappa_{\rm w} \to 0$.

The volume v_i^* is of order d_i^3 for large $d_i (> d_1)$ in terms of the hardsphere diameter d_i, while it can be negative for small $d_i (< d_1)$ such as Li^+ due to the hydration (see Sec.IIIF)[11,12,91–94]. From measurements with the overall charge neutrality, we can determine only the sum,

$$v_{\rm s}^* = v_2^* + v_3^* = 2 \epsilon_{\rm in} \nu', \tag{21}$$

where $\nu' = \partial \nu(n_{\rm w})/\partial n_{\rm w}$. This $v_{\rm s}^*$ is is smaller than the corresponding infinite-dilution partial volume $\bar{v}_{\rm s}^0$ in Eq.(47) by $2 k_B T \kappa_{\rm w}$. From experimental reports on $\bar{v}_{\rm s}^0$ in ambient water[11,74,94], $n_{\rm w} v_{\rm s}^*$ is -0.21, 0.93, 2.0, and 15 for LiF, NaCl, NaI, and $NaBPh_4$, respectively. Then, $2 n_{\rm w} \nu'$ is -3.4, 15, 32, and 240, respectively, for these salts. The $\nu(n_{\rm w})$ itself appears in the Henry constant.

For nonionic mixtures, the coefficients f_{ij} are written in terms of thermodynamic derivatives (see Eq.(26) in our recent paper[67]). Generally, f_{ij} can be expressed as

$$f_{ij}/k_B T = \delta_{ij}/\langle n_i \rangle - \int d\boldsymbol{r} c_{ij}^0(r) \quad (i, j = 1, 2, 3). \tag{22}$$

In terms of the direct correlation functions $c_{ij}(r)$, we have $c_{1j}^0(r) = c_{1j}(r)$ $(i = 1)$ and $c_{ij}^0(r) = c_{ij}(r) + (-1)^{i+j} \ell_B / r$ $(i, j = 2, 3)$[52,60,95–98]. If f_{ij} are defined in this manner, Eq.(12) can be used for general $n_{\rm s}$. In the simple case of a nonionic solute in one-component solvent, we notice $2 k_B T B_2 = (\partial \mu_2^{\rm ex}/\partial n_2)_{T,\mu_1} = U_{22}^{\rm eff}$ and $2 k_B T B_2'' = (\partial \mu_2^{\rm ex}/\partial n_2)_{T,n_1} = -k_B T \int d\boldsymbol{r} c_{22}(r)$ in Eq.(1), where $\mu_2^{\rm ex}$ is the excess solute chemical potential[49,50,67].

C. Solvent-mediated interaction and Collins' rule

Next, we derive the solvent-mediated ion-ion interaction in the long wavelength. To this end, we express the ionic term in Eq.(20) as

$$\delta\mathcal{F}_{\rm ion} = k_BT\int d\boldsymbol{r}\Big[\frac{|\delta n_2|^2+|\delta n_3|^2}{2n_{\rm s}} - \frac{\ell_B\kappa}{16n_{\rm s}}|\delta n_{\rm e}|^2\Big] + \frac{1}{2}\int_{\boldsymbol{q}}\Big[\sum_{i,j=2,3} U_{ij}^{\rm eff} n_i(\boldsymbol{q})n_j(\boldsymbol{q})^* + \frac{4\pi}{\epsilon q^2}|\rho_{\boldsymbol{q}}|^2\Big]. \quad (23)$$

In the first term, $\delta n_{\rm e} = \delta n_2 + \delta n_3$ is the ion density deviation. In the second term, we introduce the effective ionic interaction coefficients,

$$U_{ij}^{\rm eff} = U_{ij} - v_i^* v_j^*/\kappa_{\rm w} \quad (i,j=2,3), \quad (24)$$

where the first term represents the short-ranged direct interactions and the second term arises from the solvent-mediated interactions in the long wavelength limit. The second term corresponds to the second term in Eq.(1). The Coulombic term in Eq.(23) suppresses $\rho_{\boldsymbol{q}}$ at small q. Thus, in thermodynamic quantities, there appears the mean effective interaction coefficient,

$$U_{\rm eff} = \frac{1}{2}\sum_{i,j=2,3} U_{ij}^{\rm eff} = U - \frac{1}{2\kappa_{\rm m}}(v_{\rm s}^*)^2. \quad (25)$$

The second volume term in Eq.(24) is amplified by $\kappa_{\rm w}^{-1} = n_{\rm w}k_BT/\epsilon_{\rm in}$ and is very large for not very small $v_i^*v_j^*$. However, it does not appear if the solvent is treated as a homogeneous continuum[24–30]. Indeed, it is needed to explain Collins' rule[69–71]. Namely, if v_i^* and v_j^* have the same sign, it is negative leading to *solbophobic attraction* between species i and j. See (a) and (b) in Fig.1. As a result, this mechanism yields hydrophobic assembly of large solute particles[49,50,67,99]. On the other hand, for small-large ion pairs with $v_2^*v_3^* < 0$, $U_{23}^{\rm eff}$ is positive leading to non-Coulombic cation-anion repulsion, as in Fig.1(c). See Sec.IIIE and Sec.IV for more analysis on the basis of Eq.(24). Previously, some attempts were made to explain Collins' rule not using Eq.(24)[41,84,100,101].

We can also derive the second term in Eq.(24) in the mean spherical approximation (MSA) in the presence of the solvent degrees of freedom[34,98]. We also note that the interaction energy in the Flory-Huggins theory of polymer solutions corresponds to $n_{\rm w}U_{22}^{\rm eff}$ in our notation[60].

D. Fluctuation variances, charge density structure factor, and Kirwood-Buff integrals

We treat δn_i as the thermal fluctuations obeying the Gaussian distribution $\propto \exp(-\delta\mathcal{F}/k_BT)$. We can then calculate the fluctuation variances $I_{ij} = \lim_{q\to 0}\langle n_i(\boldsymbol{q})n_j(\boldsymbol{q})^*\rangle/V$, where $L^{-1} \ll q \ll \kappa$ in the limit of large L. Here, for any space-dependent variables $\hat{A}(\boldsymbol{r})$ and $\hat{B}(\boldsymbol{r})$, we write $\langle\hat{A}:\hat{B}\rangle = \lim_{q\to 0}\langle A_{\boldsymbol{q}}B_{\boldsymbol{q}}{}^*\rangle/V$,

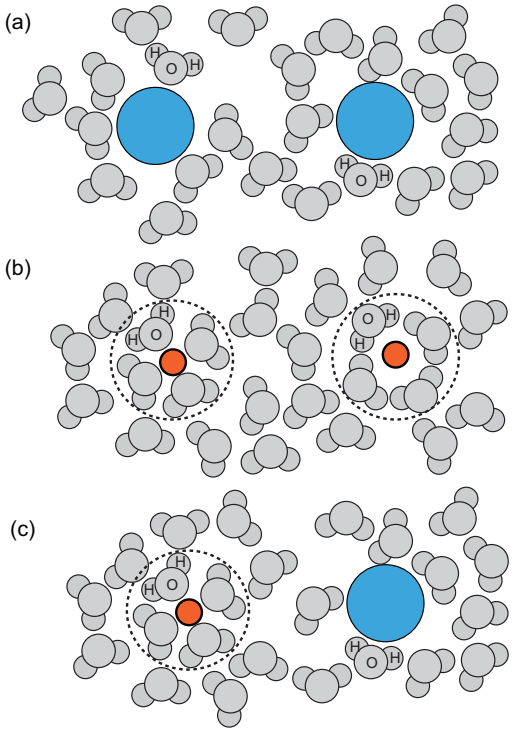


FIG. 1. (Color online) Illustration of two ions in close separation in water[69]. (a) Large-large pair with non-Coulombic attraction. Examples are CsI and CsBr. (b) Small-small ions with non-Coulombic attraction. Examples are NaF and LiF. (c) Small-large (cation-anion) pair with non-Coulombic repulsion. Examples are NaI, LiI, and $NaBPh_4$. Tendency of cation-anion association is promoted with decreasing $U_{23}^{\rm eff}$.

where $A_{\boldsymbol{q}}$ and $B_{\boldsymbol{q}}$ are the Fourier components[60]. Then, $I_{ij} = \langle n_i : n_j\rangle$. From Eq.(20) we find[67]

$$\langle\phi_v:\phi_v\rangle = k_BT/n_{\rm w}^2 f_{11} \cong \epsilon_{\rm in}/n_{\rm w}, \quad (26)$$
$$\langle\phi_v:n_i\rangle = 0 \quad (i=2,3). \quad (27)$$

As $q\to 0$, we have $\rho_{\boldsymbol{q}}\to 0$, so we find

$$I_{22} = I_{33} = I_{23} = n_{\rm s}\chi, \quad (28)$$

where $n_{\rm s}\chi$ represents the amplitude of the ion density fluctuations. See its thermodynamic expression in Eq.(44). From Eq.(18) we also find the solvent-solvent and solvent-ion fluctuation variances,

$$I_{11} = k_BT/f_{11} + (f_{12}+f_{13})^2 f_{11}^{-2} n_{\rm s}\chi, \quad (29)$$
$$I_{12} = I_{13} = -(f_{12}+f_{13})f_{11}^{-1}n_{\rm s}\chi \cong -v_{\rm s}^* n_{\rm w} n_{\rm s}/2. \quad (30)$$

In I_{11}, the first and second terms are close to $n_{\rm w}\epsilon_{\rm in}$ and $(n_{\rm w}v_{\rm s}^*)^2 n_{\rm s}/2$, respectively, for small $n_{\rm s}$. Thus, the second one is dominant for $n_{\rm s}/n_{\rm w} > 2\epsilon_{\rm in}/(v_{\rm s}^* n_{\rm w})^2$ ($\sim 4\times 10^{-4}$ for $NaPhB_4$ in water), as can be verified in experiments.

It is convenient to rewrite $\delta\mathcal{F}_{\rm ion}$ in Eq.(23) in terms of

$\delta n_{\rm e}=\delta n_2+\delta n_3$ and $\rho=e(\delta n_2-\delta n_3)$ as

$$\frac{\delta\mathcal{F}_{\rm ion}}{k_BT}=\int d\boldsymbol{r}\Big[\frac{|\delta n_{\rm e}|^2}{8n_{\rm s}\chi}+(U_{22}^{\rm eff}-U_{33}^{\rm eff})\frac{\delta n_{\rm e}\rho}{4k_BTe}\Big] +\int_{\boldsymbol{q}}\Big[1+w_\rho n_{\rm s}+\frac{\kappa^2}{q^2}\Big]\frac{|\rho\boldsymbol{q}|^2}{4e^2n_{\rm s}}. \quad (31)$$

The inverse χ^{-1} in the first term depends on $n_{\rm s}$ as

$$\chi^{-1}=2-\ell_B\kappa/2+2n_{\rm s}U_{\rm eff}/k_BT. \quad (32)$$

The coefficient w_ρ in the second term arises from asymmetry between the cations and the anions as

$$w_\rho=(U_{22}^{\rm eff}+U_{33}^{\rm eff}-2U_{23}^{\rm eff})/2k_BT =[U_{22}+U_{33}-2U_{23}-(v_2^*-v_3^*)^2/2\kappa_{\rm w}]/2k_BT. \quad (33)$$

From Eq.(31) the structure factor for the charge density fluctuations $\rho_{\boldsymbol{q}}$ for $q\ll\kappa$ is given by[52,95–97]

$$S_{\rho\rho}(q)=\langle|\rho_{\boldsymbol{q}}|^2\rangle/V=2e^2n_{\rm s}/[1+w_\rho n_{\rm s}+\kappa^2/q^2]. \quad (34)$$

The cross term $\propto\rho\delta n_{\rm e}$ in Eq.(31) gives a higher-order term($\propto n_{\rm s}^2$) in the denominator in Eq.(34). For $1+w_\rho n_{\rm s}>0$, the screening length is given by

$$\xi_\rho=\kappa^{-1}\sqrt{1+w_\rho n_{\rm s}}, \quad (35)$$

which is valid for $\kappa d_1\ll1$ or for $n_{\rm s}\ll0.02n_{\rm w}\sim1$ mol/L with $d_1=3$Å in water. In Sec.IV, we shall see that w_ρ is negative and $|w_\rho|$ increases with increasing the cation-anion asymmetry (see Fig.9(d) and Eq.(100)). Thus, $\xi_\rho\kappa$ decreases with increasing $n_{\rm s}$ for small $n_{\rm s}$ as observed[102]. A similar decrease was derived in the MSA scheme[26,27] and in phenomenoological theories[96,103] However, ξ_ρ increases with increasing $n_{\rm s}$ above 1 mol/L[102–104], as a remarkable effect beyond the scope of this paper.

In Eq.(28) the cations and the anions are indistinguishable. Thus, we define the Kirkwood-Buff integrals (KBIs)[47] for the water density n_1 and the ion density $n_{\rm e}=n_2+n_3$[38,43,44,46,105,106]. Then, Eqs.(28)-(30) give the ion-ion and ion-solvent KBIs:

$$G_{\rm ss}=\langle n_{\rm e}:n_{\rm e}\rangle/4n_{\rm s}^2-1/2n_{\rm s}=(2\chi-1)/2n_{\rm s}, \quad (36)$$
$$G_{\rm ws}=\langle n_1:n_{\rm e}\rangle/2n_{\rm w}n_{\rm s}=-\chi(f_{12}+f_{13})/n_{\rm w}f_{11}. \quad (37)$$

Thus, as $n_{\rm s}\to0$, we have $G_{\rm ss}\propto n_{\rm s}^{-1/2}$ and $G_{\rm ws}\cong-v_{\rm s}^*/2$. Note that $G_{\rm ws}$ represents exclusion (adsorption) of water molecules around an ion pair for positive (negative) $v_{\rm s}^*$.

In their simulation, Naleem *et al.*[46] found growth of $G_{\rm ss}$ at low densities of $CaCl_2$. Here, we readily derive $G_{\rm ss}=Z_+Z_-\ell_B\kappa/4\langle n_{\rm e}\rangle+\cdots$, where the cations and anions have changes Z_+e and $-Z_-e$, respectively,

III. THERMODYNAMICS OF ELECTROLYTES

In this section, we study the electrolyte thermodynamics using the Helmholtz free energy $F=\lim_{\Lambda\to0}\mathcal{F}$. We give remarks on previous research. (i) Pitzer[18] used the Gibbs free energy G. In Appendix B, a scheme of G will be given. (ii) In many papers[1,28,29,79–87], *associated ion pairs* are treated as dipoles coexisting with unbound ions. However, they appear as ion clusters with finite lifetimes in water. In Appendix A, we will show how our theory is modified by such dipoles at small $n_{\rm s}$. (iii) Since McQuarrie's paper on fused salts[107], many authors[28–32,108] discussed a gas-liquid phase transition of the ions due to $f_{\rm DH}$ in Eq.(5) without solvent-ion interactions, where a_2 and a_3 are the ion hardsphere diameters.

A. Free energy, chemical potentials, pressure, and thermodynamic derivatives

From Eqs.(3) and (7)-(9). F is expressed as

$$F/V=f_{\rm w}(n_{\rm w})+2k_BT[\ln(n_{\rm s}\lambda^3)-1+\nu(n_{\rm w})]n_{\rm s} -k_BT\kappa^3/12\pi+Un_{\rm s}^2. \quad (38)$$

where $\lambda=\sqrt{\lambda_2\lambda_3}$. This is the expression up to order $n_{\rm s}^2$. We introduce the solvent chemical potential $\mu_{\rm w}$ and the salt one $\mu_{\rm s}$ (per cation-anion pair) from $d(F/V)=\mu_{\rm w}dn_{\rm w}+\mu_{\rm s}dn_{\rm s}$ at fixed T. The pressure $p=n_{\rm w}\mu_{\rm w}+n_{\rm s}\mu_{\rm s}-F/V$ satisfies the Gibbs-Duhem relation,

$$dp=n_{\rm w}d\mu_{\rm w}+n_{\rm s}d\mu_{\rm s}. \quad (39)$$

From Eq.(38), $\mu_{\rm w}$, $\mu_{\rm s}$, and p are expanded as

$$\mu_{\rm w}=\mu_{\rm w}^0(n_{\rm w})+k_BT[2\nu'+\ell_B\kappa\epsilon'/\epsilon]n_{\rm s}+U'n_{\rm s}^2, \quad (40)$$
$$\mu_{\rm s}=k_BT[2\ln(n_{\rm s}\lambda^3)+2\nu-\ell_B\kappa]+2Un_{\rm s}, \quad (41)$$
$$p=p_{\rm w}^0(n_{\rm w})+2k_BT(1+n_{\rm w}\nu')n_{\rm s}+(U+n_{\rm w}U')n_{\rm s}^2 -k_BT\kappa^3(1-3n_{\rm w}\epsilon'/\epsilon)/24\pi, \quad (42)$$

where $U'=\partial U(n_{\rm w})/\partial n_{\rm w}$. We define the chemical potential $\mu_{\rm w}^0=\partial f_{\rm w}(n_{\rm w})/\partial n_{\rm w}$ and the pressure $p_{\rm w}^0=n_{\rm w}\mu_{\rm w}^0-f_{\rm w}$ for pure solvent at density $n_{\rm w}$. They vary significantly even for a small change of $n_{\rm w}$ from $n_{\rm w}\partial\mu_{\rm w}^0/\partial n_{\rm w}=\partial p_{\rm w}^0/\partial n_{\rm w}=1/n_{\rm w}\kappa_{\rm w}=k_BT/\epsilon_{\rm in}$.

Next, the second derivatives of F/V are written as

$$f_{KM}=\frac{\partial^2(F/V)}{\partial n_M\partial n_K}=\frac{\partial\mu_K}{\partial n_M}\quad(K,M={\rm w,s}). \quad (43)$$

Here, $f_{\rm ww}=f_{11}$, $f_{\rm ws}=\sum_{i=2,3}f_{1i}$, and $f_{\rm ss}=\sum_{i,j=2,3}f_{ij}$ in terms of f_{ij} in Eq.(13). Note that the inverse matrix of $\{f_{KM}\}$ is given by $\{\partial n_K/\partial\mu_M\}$, where $n_{\rm w}$ and $n_{\rm s}$ are functions of $\mu_{\rm w}$ and $\mu_{\rm s}$. The elements of this inverse matrix are the fluctuation variances among δn_1 and $(\delta n_2+\delta n_3)/2$ divided by k_BT. Thus, Eq.(28) gives

$$n_{\rm s}\chi=k_BT(\partial n_{\rm s}/\partial\mu_{\rm s})_{\mu_{\rm w},T}=k_BT/[f_{\rm ss}-f_{\rm ws}^2/f_{\rm ww}]. \quad (44)$$

Let us examine the isothermal compressibility $\kappa_T=-V^{-1}\partial V/\partial p$, where $N_{\rm w}=Vn_{\rm w}$, $N_{\rm s}=Vn_{\rm s}$, and T are

fixed in the pressure derivative. In terms of f_{KM} in Eq.(43), its inverse is expressed as

$$\kappa_T^{-1} = \sum_{K=\mathrm{w,s}} n_K \frac{\partial p}{\partial n_K} = \sum_{K,M=\mathrm{w,s}} n_K n_M f_{KM} = \kappa_\mathrm{w}^{-1} + 2k_BT(1 + 2n_\mathrm{w}\nu' + n_\mathrm{w}^2\nu'')n_\mathrm{s}, \quad (45)$$

where the DH term is of order $n_\mathrm{s}^{3/2}$ (not written here). For NaCl in water, Millero *et al.*[109] found that $(\kappa_\mathrm{w}/\kappa_T - 1)/n_\mathrm{s}$ tends to a constant as $n_\mathrm{s} \to 0$, which was $7n_\mathrm{w}^{-1}$ at $T = 303$ K. Thus, $n_\mathrm{w}\nu''/\nu' \sim 5$ from Eq.(45).

The thermodynamic partial volumes are defined by $\bar{v}_K = (\partial V/\partial N_K)_{T,p,N_M}$ $(M \neq K)$. Since V and $N_K = Vn_K$ are extensive, they satisfy the sum rule $\bar{v}_\mathrm{w}n_\mathrm{w} + \bar{v}_\mathrm{s}n_\mathrm{s} = 1$. At fixed T, the relation $dV = \sum_K \bar{v}_K dN_K - V\kappa_T dp$ then holds yielding $\kappa_T dp = \sum_K \bar{v}_K dn_K$ and

$$\bar{v}_\mathrm{s} = \kappa_T(\partial p/\partial n_\mathrm{s})_{T,n_\mathrm{w}}, \quad \bar{v}_\mathrm{w} = \kappa_T(\partial p/\partial n_\mathrm{w})_{T,n_\mathrm{s}}. \quad (46)$$

Here, $\bar{v}_\mathrm{s}$ is defined for a cation-anion pair. As $n_\mathrm{s} \to 0$, Eqs.(42) and (46) give the infinite-dilution limit,

$$\bar{v}_\mathrm{s}^0 = \lim_{n_\mathrm{s}\to 0} \bar{v}_\mathrm{s} = 2\epsilon_\mathrm{in}(\nu' + n_\mathrm{w}^{-1}) = v_\mathrm{s}^* + 2k_BT\kappa_\mathrm{w}, \quad (47)$$

where v_s^* appears in Eq.(21). The difference $\bar{v}_\mathrm{s}^0 - v_\mathrm{s}^* = 2k_BT\kappa_\mathrm{w}$ stems from the ionic partial pressure $2k_BTn_\mathrm{s}$ and is $0.12n_\mathrm{w}^{-1}$ in ambient water. It is relevant for small-small ion pairs; for example, $n_\mathrm{w}\bar{v}_\mathrm{s}^0 = -0.09$ and $n_\mathrm{w}v_\mathrm{s}^* = -0.21$ for NaF. The values of $\bar{v}_\mathrm{s}^0$ are listed for various salts in the experimental reports[11,74,94]. Many authors[11,12,91–93] introduced single-ion volumes, which are $v_i^* + k_BT\kappa_\mathrm{w}$ in our notation.

B. Salt-doping and apparent partial volumes

In experiments of salt-doping, it follows an *apparent* partial volume v_s^ap from the space-filling relation[1,11,20,21]:

$$n_\mathrm{w}/n_\mathrm{w}^0 + v_\mathrm{s}^\mathrm{ap}n_\mathrm{s} = 1, \quad (48)$$

where n_w^0 is the initial solvent density. The salt density is increased from 0 to n_s. The simplest example is to fix the volume V, where $n_\mathrm{w} = n_\mathrm{w}^0$, $v_\mathrm{s}^\mathrm{ap} = 0$, and $\ln\gamma_\pm = -\ell_B\kappa/2 + Un_\mathrm{s}/k_BT$ from Eq.(41) (see Eq.(54) for the definition of $\gamma_\pm$).

As a well-known doping method, let a 1:1 electrolyte region be in osmotic equiibrium with a pure solvent region, which are separated by a semipermeable membrane[51,67,110]. The solvent chemical potential μ_w is commonly given by $\mu_\mathrm{w}(n_\mathrm{w}, n_\mathrm{s}) = \mu_\mathrm{w}^0(n_\mathrm{w}^0)$. From $d\mu_\mathrm{w} = \sum_K f_{\mathrm{w}K}dn_\mathrm{K} = 0$, we set up the equation,

$$dn_\mathrm{w}/dn_\mathrm{s} = (\partial n_\mathrm{w}/\partial n_\mathrm{s})_{\mu_1,T} = -f_\mathrm{ws}/f_\mathrm{ww}. \quad (49)$$

From Appendix C, we find the apparent partial volume,

$$v_\mathrm{s}^\mathrm{ap} = v_\mathrm{s}^*(n_\mathrm{w}^0) + (\epsilon'/\epsilon)\epsilon_\mathrm{in}\ell_B\kappa + n_\mathrm{s}\partial U_\mathrm{eff}/\partial p. \quad (50)$$

We also calculate the osmotic pressure $\Pi = p(n_\mathrm{w}, n_\mathrm{s}) - p_\mathrm{w}^0(n_\mathrm{w}^0)$. From $d\Pi = n_\mathrm{s}d\mu_\mathrm{s}$ and Eq.(44), we find

$$d\Pi/dn_\mathrm{s} = n_\mathrm{s}\sum_K f_{\mathrm{s}K}(dn_\mathrm{K}/dn_\mathrm{s}) = k_BT/\chi, \quad (51)$$

which holds for general n_s. We integrate Eq.(51) using Eq.(32) to obtain

$$\Pi/2k_BTn_\mathrm{s} = 1 - \ell_B\kappa/6 + U_\mathrm{eff}n_\mathrm{s}/2k_BT. \quad (52)$$

C. Isobaric equilibrium at fixed p

Most salt-doping experiments have been performed at a constant pressure p[1,13,14,19]. In this case, the salt number is increased from 0 to $N_\mathrm{s} = Vn_\mathrm{s}$ with

$$p(n_\mathrm{w}, n_\mathrm{s}) = p_\mathrm{w}^0(n_\mathrm{w}^0), \quad (53)$$

where n_w^0 is the initial solvent density. We can also fix the total solvent number $N_\mathrm{w} = Vn_\mathrm{w} = V_0n_\mathrm{w}^0$, where V_0 is the initial volume. Then, Eq.(48) becomes $V = V_0 + v_\mathrm{s}^\mathrm{ap}N_\mathrm{s}$. This isobaric v_s^ap has been measured, where the product $\phi_\mathrm{v} = v_\mathrm{s}^\mathrm{ap}N_\mathrm{A}$ is called the apparent molal volume with N_A being the Avogadro number. In Eq.(B3) in Appendix B, $\bar{v}_\mathrm{s}$ will be expressed in terms of this v_s^ap.

We define the *molal* mean activity coefficient $\gamma_\pm$ by expressing the salt chemical potential μ_s in Eq.(41) as

$$\mu_\mathrm{s}/2k_BT = \nu(n_\mathrm{w}^0) + \ln(\lambda^3\gamma_\pm N_\mathrm{s}/V_0). \quad (54)$$

We also introduce the *molar* mean activity coefficient[1],

$$y_\pm = (V/V_0)\gamma_\pm = (1 + v_\mathrm{s}^\mathrm{ap}N_s/V_0)\gamma_\pm. \quad (55)$$

Then, $\gamma_\pm N_\mathrm{s}/V_0 = n_\mathrm{s}y_\pm$ in Eq.(54). Setting $\nu(n_\mathrm{w}) \cong \nu(n_\mathrm{w}^0) - \nu' n_\mathrm{w}^0\bar{v}_\mathrm{s}^0 n_s$ in Eq.(41), we obtain

$$\ln\gamma_\pm = -\ell_B\kappa/2 + \tilde{U}_\mathrm{eff}n_\mathrm{s}/k_BT. \quad (56)$$

At fixed p we use the coefficient $\tilde{U}_\mathrm{eff}$ defined by

$$\tilde{U}_\mathrm{eff} = U - (\bar{v}_\mathrm{s}^0)^2/2\kappa_\mathrm{w} = U_\mathrm{eff} - k_BT(v_\mathrm{s}^* + \bar{v}_\mathrm{s}^0), \quad (57)$$

where v_s^* in Eq.(25) is replaced by $\bar{v}_\mathrm{s}^0$ in Eq.(47). It will also appear in the Gibbs free energy in Appendix B. Note that $\tilde{U}_\mathrm{eff}/k_BT$ can be known from the data of $(\ln\gamma_\pm + \ell_B\kappa/2)/n_\mathrm{s}$, which is slightly negative for LiF $(\sim -2/n_\mathrm{w})^2$, positive for the the other alkali halide salts, and is largely negative for $NaPBh_4$ $(\sim -60/n_\mathrm{w})$[73].

We also have $dp = \sum_{K,M}(n_Kf_{KM})dn_M = 0$ from Eq.(39). Using Eq.(43), we can set up the equation,

$$\frac{dn_\mathrm{w}}{dn_\mathrm{s}} = \left(\frac{\partial n_\mathrm{w}}{\partial n_\mathrm{s}}\right)_{p,T} = -\frac{f_\mathrm{ws}}{f_\mathrm{ww}} - \frac{k_BT/\chi}{n_\mathrm{w}f_\mathrm{ww} + n_\mathrm{s}f_\mathrm{ws}}. \quad (58)$$

Here, the second term is $(\partial n_\mathrm{s}/\partial\mu_\mathrm{w})_{n_\mathrm{s},T}(\partial\mu_\mathrm{w}/\partial n_\mathrm{s})_{p,T}$. From Appendix C, we find the aparent partial volume,

$$v_\mathrm{s}^\mathrm{ap} = \bar{v}_\mathrm{s}^0(n_\mathrm{w}^0) + (\epsilon'/\epsilon - 1/3n_\mathrm{w})\epsilon_\mathrm{in}\ell_B\kappa + hn_\mathrm{s}. \quad (59)$$

The second term is the DH part derived by Redlich[20,21]. The h is called the deviation constant and has been measured (see Table IV in Sec.IV)[11,23,74]. It is expressed as

$$h = \kappa_{\rm w}\tilde{U}_{\rm eff} + \partial\tilde{U}_{\rm eff}/\partial p. \tag{60}$$

We can also derive Eqs.(59) and (60) by expanding $p(n_{\rm w}, n_{\rm s})$ in Eq.(42) with respect to $\delta n_{\rm w} = n_{\rm w} - n_{\rm w}^0$.

The derivative $d\mu_{\rm w}/dn_{\rm s} = (\partial\mu_{\rm w}/\partial n_{\rm s})_{p,T}$ is given by the second term in Eq.(58) multiplied by $f_{\rm ww}$. Its integration gives $\mu_{\rm w}$, leading to $\mu_{\rm w} = \mu_{\rm w}^0 - 2k_BTn_{\rm s}/n_{\rm w}^0 + \cdots$ for small $n_{\rm s}$, where $\mu_{\rm w}^0 = f_{\rm w}'(n_{\rm w}^0)$ is the initial chemical potential of pure solvent. Thus, we define

$$\varphi = [\mu_{\rm w}^0(n_{\rm w}^0) - \mu_{\rm w}(n_{\rm w}, n_{\rm s})]/(2k_BTn_{\rm s}/n_{\rm w}). \tag{61}$$

After some calculations we obtain the expansion,

$$\varphi = 1 - \ell_B\kappa/6 + \tilde{U}_{\rm eff}n_{\rm s}/2k_BT. \tag{62}$$

This φ is called the osmotic coefficient as well as $\Pi/2k_BTn_{\rm s}$ in Eq.(52)[1,19], but the linear term($\propto n_{\rm s}$) in Eq.(52) is larger than that in Eq.(62) by $(\bar{v}_{\rm s}^0 - k_BT\kappa_{\rm w})n_{\rm s}$.

From $n_{\rm s}d\mu_{\rm s}/dn_{\rm s} = -n_{\rm w}d\mu_{\rm w}/dn_{\rm s}$, we also find[105]

$$1 + n_{\rm s}(\partial \ln y_\pm/\partial n_{\rm s})_{p,T} = 1/[1 + 2n_{\rm s}(G_{\rm ss} - G_{\rm ws})], \tag{63}$$

with the aid of Eqs.(54) and (55). Here, $G_{\rm ss}$ and $G_{\rm ws}$ are the KBIs in Eqs.(36) and (37), which satisfy $1+2n_{\rm s}(G_{\rm ss} - G_{\rm ws}) = 2\chi(1+n_{\rm s}f_{\rm ws}/n_{\rm w}f_{\rm ww})$ from Eq.(44). This relation has been used in simulations to calculate $y_\pm$[38,43,44,46].

We make some comments. (i) In Appendix B, we will derive Eqs.(59), (60), and (62) from the Gibbs free energy. (ii) Bernard *et al.*[19] related φ and Π by $\varphi = (1 - \bar{v}_{\rm s}^0 n_{\rm s})\Pi/2k_BTn_{\rm s}$, where $\bar{v}_{\rm s}^0$ should be replaced by $\bar{v}_{\rm s}^0 - k_BT\kappa_{\rm w}$ in our theory. (iii) The behavior $\propto \sqrt{n_{\rm s}}$ of the first corrections in $\ln\gamma_\pm$ and φ is the DH limiting law, which was known empirically before the DH theory[13,14].

D. Expressions in extended Debye-Hückel theory

With increasing $n_{\rm s}$, the lowest DH terms in Eqs.(56), (59), and (62) increase as $\sqrt{n_{\rm s}}$, while the Debye length κ^{-1} decreases toward the minimum length (a_2 or a_3). However, $f_{\rm DH}$ in Eq.(5) is suppressed with increasing $a_i\kappa$. Due to this reason, many authors used *extended* DH expressions to explain experimental data[1,2,15,16,18].

We thus rewrite $\gamma_\pm$ in Eq.(56) and φ in Eq.(62) as[15,16]

$$\ln\gamma_\pm = -\frac{1}{4}\ell_B\kappa\sum_{i=2,3}\frac{1}{1+a_i\kappa} + bn_{\rm s}, \tag{64}$$

$$\varphi = 1 - \frac{1}{12}\ell_B\kappa\sum_{i=2,3}\sigma(a_i\kappa) + \frac{1}{2}b'n_{\rm s}, \tag{65}$$

where $\sigma(x) = 3[x + x/(1+x) - 2\ln(1+x)]/x^3$ and $\sigma(x) = 1 - 3x/2 + \cdots$ for $x \ll 1$. For small $a_i\kappa$ we compare Eqs.(64) and (65) and Eqs.(56) and (62) to find

$$b = b' \cong \tilde{V}_{\rm eff}/k_BT. \tag{66}$$

TABLE I. Data of mean activity coefficient $\gamma_\pm$ and osmotic coefficient φ for alkali halide salts at molality 0.5 in ambient water[111]. The latter are in (). LiF is insoluble at this density.

	F^-	Cl^-	Br^-	I^-
Li^+		0.739 (0.964)	0.754 (0.970)	0.824 (1.008)
Na^+	0.633 (0.887)	0.681 (0.921)	0.697 (0.932)	0.722 (0.950)
K^+	0.670 (0.916)	0.649 (0.900)	0.658 (0.906)	0.676 (0.918)
Rb^+	0.701 (0.939)	0.633 (0.891)	0.630 (0.889)	0.627 (0.887)
Cs^+	0.721 (0.946)	0.607 (0.873)	0.605 (0.870)	0.601 (0.868)

TABLE II. Coefficient b in Eq.(64) and $\tilde{V}_{\rm eff}/k_BT$ from Eqs.(56) and (67) in units of d_1^3. The latter are in (). Use is made of data on the mean activity coefficient for alkali halide salts at molality 0.02 for LiF[2] and 0.1 for the others[111].

	F^-	Cl^-	Br^-	I^-
Li^+	-68.0 (-70.4)	22.1 (11.5)	28.3 (17.8)	43.7 (33.2)
Na^+	2.1 (-8.4)	14.2 (3.6)	17.4 (6.79)	22.1 (11.5)
K^+	9.4 (-1.2)	5.4 (-5.2)	7.8 (-2.8)	11.8 (1.2)
Rb^+	15.0 (4.4)	-0.3 (-10.9)	-1.1 (-11.7)	-2.0 (-12.5)
Cs^+	24.4 (13.9)	-8.5 (-19.1)	-7.7 (-18.3)	-10.2 (-20.7)

Here, using $\tilde{U}_{\rm eff}$ in Eq.(57) and $u_{ij}^{\rm ex}$ in Eq.(6), we define

$$\tilde{V}_{\rm eff} = \tilde{U}_{\rm eff} - \frac{1}{2}\sum_{i,j}u_{ij}^{\rm ex} = \tilde{U}_{\rm eff} - 2\pi k_BT\ell_B^2(a_2 + a_3), \tag{67}$$

In Appendix D, we will present extended DH forms for χ^{-1} in Eq.(32) and $v_{\rm s}^{\rm ap}$ in Eq.(59).

Guggenheim and Turgeon[15,16] nicely fitted Eqs.(64) and (65) to 1:1 electrolyte data with $b = b'$ and $a_2 = a_3 = 3$Å. They used many data points for each salt. For their choice of a_i, the relation $a_i\kappa \cong \sqrt{m}$ holds, where m is the molality. Many authors[1,2,18] took this *practical* approach with empirical $b = b'$.

E. Experimental trends and Collins' rule

Table I gives $\gamma_\pm$ and φ for alkali halide salts at molality 0.5 in ambient water[111]. We notice the following. (i) For F^-, $\gamma_\pm$ and φ increase with increasing the cation size. For the other anions, they are smaller for larger cations. (ii) For small cations Li^+ and Na^+, $\gamma_\pm$ and φ increase as the anion size increases. For large cations Rb^+ and Cs^+, the tendency is reversed. (iii) For K^+, they are close for all the anions. Thus, K^+ ions have a marginal size.

Table II gives b in Eq.(64) and $\tilde{V}_{\rm eff}/k_BT$ from Eqs.(56) and (67) in units of $d_1^3 = 0.9n_{\rm w}^{-1}$, where $a_2 = a_3 = 3$Å. We use data of $\gamma_\pm$ at molality 0.02 for LiF[2] and 0.1 for the others[111]. The molality 0.1 is not very small with $a_i\kappa = 0.31$, so the numbers of b are larger than those of $\tilde{V}_{\rm eff}/k_BT$ by 10. Here, $n_{\rm w}U_{\rm eff}/k_BT$ is about -5 for LiF and is between 50 and 110 for the others. These ion-size-dependences are the same as those in Table I. In Fig.2,

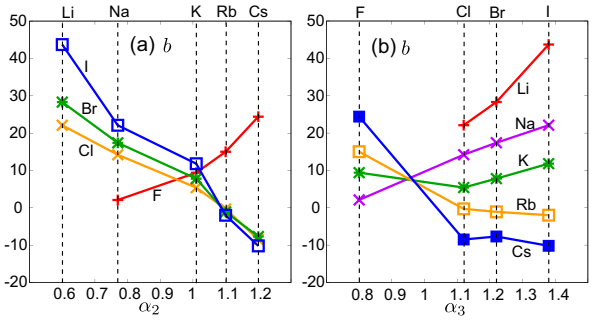


FIG. 2. (Color online) Coefficient b in Table II vs radius ratios (α_2 for cations in (a) and α_3 for anions in (b)), where b appears in the activity coefficient in Eq.(64). Here, Collins' rule holds.

to illustrate this common trend, we plot b in Table II vs $\alpha_i = 2R_i^{\rm S}/d_1$ ($i = 2$ for cations and $i = 3$ for anions) with $d_1 = 3$ Å, using the crystal radii $R_i^{\rm S}$ by Shannon[112].

Collins[69] noticed the same pattern in the solubility of alkali halide salts in water as those in Tables I and II. That is, salts of large-small pairs are highly soluble, whereas salts of large-large or small-small pairs are much less soluble. In fact, the solubility is 0.05, 1, and 20 mol/L for LiF, NaF, and LiCl[69,113], respectively. He argued that large-small pairs remain apart but cation-anion pairs with comparable sizes tend to be closely connected. Note that the salt solubility is correlated with $U_{23}^{\rm eff}$.

For $NaBPh_4$[73], the numbers from the two methods in Table II are -120.7 (-130.5) at molality 0.09, leading to $U_{\rm eff} \sim \tilde{U}_{\rm eff} \sim -60 k_BT/n_{\rm w}$. For this salt, the two terms in Eq.(25) are both about $1800 k_BT/n_{\rm w}$ from $v_3^* \cong 15/n_{\rm w}$[74] and their difference $U_{\rm eff}$ is much smaller ($\sim 3\%$).

If the cations and/or the anions are large, $U_{\rm eff}$ is largely negative from Eq.(25). In such cases, a thermodynamic instability occurs[67] if $n_{\rm s}$ exceeds a spinodal density $n_{\rm s}^{\rm spi}$ determined by $\chi^{-1} = 0$. For $n_{\rm w}|U_{\rm eff}|/k_BT \gg 20$ in ambient water, the DH term is negligle in Eq.(32), so

$$n_{\rm s}^{\rm spi} \sim k_BT/|U_{\rm eff}|. \tag{68}$$

For $NaBPh_4$, $n_{\rm s}^{\rm spi}$ is on the order of its solubility ($= 1.4$ mol/L$= 0.025 n_{\rm w}$). In this instability, the ions aggregate as solvophobic spinodal decomposition[30,60,114]. However, ion association can trigger precipitate formation in metastable solutions, which is the case for alkali halide salts in water[115–117]. For LiF, its solubility ($= 0.14$ mol/L $= 0.002 n_{\rm w}$) is exceptionally small ($\ll n_{\rm s}^{\rm spi}$). On the other hand, in aqueous mixture solvents, phase separation can be induced even at slight doping of a strongly hydrophilic salt[118,119].

F. Electrostriction from Born theory

Let us consider the hydration part of the ion chemical potentials due to the ion-dipole interaction, written as $k_BT\nu_i^{\rm B}$. In the simple continuum theory[10–12], it is the integral of the electrostatic energy density $\epsilon E(r)^2/8\pi$ in the region $r > R_i$, where $E(r) = \pm e/\epsilon r^2$ is the electric field at distance r from the ion and R_i is called the Born radius. Using the bulk dielectric constant ϵ, we find

$$k_BT\nu_i^{\rm B}(n_{\rm w}) = (e^2/2R_i)(1/\epsilon - 1) \quad (i = 2, 3), \tag{69}$$

where the contribution without polarization is subtracted. We assume that R_i is independent of $n_{\rm w}$, while ϵ depends on it as in Eq.(17). From Eq.(19) the electrostriction part of v_i^* is given by

$$v_i^{\rm B} = \epsilon_{\rm in} d\nu_i^{\rm B}/dn_{\rm w} = -\epsilon_{\rm in}\ell_B\epsilon'/(2\epsilon R_i), \tag{70}$$

which is rewritten as $(e^2/2R_i)\partial\epsilon^{-1}/\partial p$, as was first derived by Drude and Nernst[120]. We also assume homogeneity of the local solvent chemical potential around each ion[53,121]. We then find the solvent density increase,

$$\delta n_{\rm w}(r) = n_{\rm w}^2\kappa_{\rm w}\epsilon' E(r)^2/8\pi = -n_{\rm w} v_i^{\rm B} R_i/(4\pi r^4), \tag{71}$$

whose integration ($r > R_i$) is $-n_{\rm w} v_i^{\rm B}$ as it should be the case. In ambient water, we have $n_{\rm w} v_i^{\rm B} \cong -0.24/R_i$ and $\delta n_{\rm w}(r)/n_{\rm w} \cong 0.51/r^4$ with R_i and r in units of Å. where $\delta n_{\rm w}(r)$ grows unrealistically around small ions.

The Born expressions are very approximate. In water, dielectric saturation occurs and ϵ nonlinearly decreases in the immediate vicinity of ions[93,122] In fact, Eq.(70) cannot be well fitted to the electrostriction data[12] if R_i is equated with the radius calculated from the crystal lattice constants[112]. For example, Mazzini and Craig[94] estimated the electrostriction part of $\bar{v}_{\rm s}^0$ in Eq.(47) as -13.0 cm^3/mol $= -0.72/n_{\rm w}$ for NaCl. This size is twice as large as that from Eq.(70) if we set $R_2 \sim 1$Å for Na^+ and $R_3 \sim 2$Å for Cl^-. Thus, if we use the Born theory with the bulk ϵ to explain the electrostriction data, we should treat R_i as a short, effective radius (see Eq.(86)).

In addition, the static dielectric constant ϵ depends on $n_{\rm s}$ as $\epsilon(n_{\rm w}, n_{\rm s})/\epsilon(n_{\rm w}, 0) \cong 1 - g_1 n_{\rm s}$, where $g_1 n_{\rm w} \sim 10$ for alkali hallides[40,123–125]. This indicates that $1/\epsilon$ in Eq.(69) should be changed to $(1 + g_1 n_{\rm s})/\epsilon(n_{\rm w}, 0)$, which yields an additional positive contribution to $U_{\rm eff}$[126]. In this paper, we neglect such an indirect repulsive interaction.

IV. MODEL CALCULATIONS

To make numerical analysis, we combine the MCSL model[61], the attractive part of the Lennard-Jones (LJ) potentials[127], and the Born chemical potentials[10]. Introducing the hardsphere diameters d_1, d_2, and d_3 for the solvent, the cations, and the anions, respectively, we vary the diameter ratios,

$$\alpha_i = d_i/d_1. \tag{72}$$

The steric interaction sensitively depends on whether α_2 and α_3 are larger or smaller than 1. In the following, large and small ions are roughly those with $\alpha_i \gtrsim 1.2$ and $\alpha_i \lesssim 0.8$, respectively.

A. Local free energy density f

The free energy density f in Eq.(3) is given by

$$f = k_BT \sum_{i=1,2,3} n_i[\ln(n_i\lambda_i^3)-1]+f_{\rm DH}+f_{\rm h}+f_{\rm a}+f_{\rm B}, \quad (73)$$

where the first term is the ideal-gas part and $f_{\rm DH}$ is the DH free energy density in Eq.(5). The third term $f_{\rm h}$ is the MCSL steric part written up to second order in n_2 and n_3 as

$$f_{\rm h} = f_{\rm h}^0(n_1) + k_BT \sum_{i=2,3} \nu_i^h n_i + \frac{1}{2} \sum_{i,j=2,3} U_{ij}^h n_i n_j, \quad (74)$$

where f_h^0 is given by the Carnahan-Starling form[64],

$$f_h^0 = k_BT n_1(4-3\eta_1)\eta_1/(1-\eta_1)^2, \quad (75)$$

with $\eta_1 = v_1 n_1$ with $v_1 = \pi d_1^3/6$ being the hardcore volume of a solvent particle. See Appendix E for expressions of ν_i^h and U_{ij}^h. The fourth term $f_{\rm a}$ represents the attractive interaction assuming the van der Waals form,

$$f_{\rm a} = -\frac{1}{2} \sum_{i,j=1,2,3} w_{ij} n_i n_j. \quad (76)$$

The coefficients w_{ij} $(i,j=1,2,3)$ are constants given by

$$w_{ij} = (4\sqrt{2}\pi/9)\epsilon_{ij}(d_i+d_j)^3, \quad (77)$$

where ϵ_{ij} are interaction energies in the LJ potentials[127]. From Eq.(69) the hydration part $f_{\rm B}$ is written as

$$f_{\rm B} = k_BT \sum_{i=2,3} \nu_i^{\rm B}(n_1) n_i. \quad (78)$$

The free energy density of pure solvent is given by[128]

$$f_{\rm w}(n_1) = k_BT n_1(\ln(n_1\lambda_1^3)-1] + f_h^0(n_1) - \frac{1}{2} w_{11} n_1^2. \quad (79)$$

The incompressibility parameter $\epsilon_{\rm in}$ in Eq.(10) becomes

$$\epsilon_{\rm in} = [1/\epsilon_{\rm in}^h - n_1 w_{11}/k_BT]^{-1}, \quad (80)$$

where $\epsilon_{\rm in}^h$ is the hardcore part. Its iverse is written as[64]

$$1/\epsilon_{\rm in}^h = 1 + 2\eta_1(4-\eta_1)/(1-\eta_1)^4, \quad (81)$$

where the second term grows for $\eta_1 \gtrsim 0.5$. For water, the hydrogen bonding yields a high critical temperature (647.1K), so we need a relatively large w_{11} to make the phase diagram from $f_{\rm w}$ mimic that of water[67]. Thus, we introduce the attraction parameter of the solvent,

$$w_{\rm a} = \epsilon_{\rm in}/\epsilon_{\rm in}^h - 1 = \epsilon_{\rm in} n_1 w_{11}/k_BT, \quad (82)$$

which is of order 1 for ambient water as its speciality.

We set d_1 and ϵ_{11} in $f_{\rm w}$ in Eq.(79) equal to

$$d_1 = 3\,\text{Å}, \quad \epsilon_{11}/k_B = 412.72\,\text{K}. \quad (83)$$

For ambient water ($T = 300\,$K and $p = 1\,$atm), these give the experimental compressibility $\kappa_{\rm w} = 4.5\times10^{-4}\,\text{MPa}^{-1}$. We also obtain $n_1 = 0.857/d_1^3 = 31.7\text{nm}^{-3}$, which is slightly smaller than the experimental one $= 33.3\ \text{nm}^{-3}$. Then, $1/\epsilon_{\rm in}^h = 35.5$ and $n_1 w_{11}/k_BT = 18.6$. Thus,

$$\eta_1 = v_1 n_1 = 0.448, \quad \epsilon_{\rm in} = 0.059, \quad w_{\rm a} = 1.10. \quad (84)$$

Previously[65–67], we assumed $\epsilon_{11}/k_B = 588.76\,$K to obtain the saturated vapor pressure of water ($= 0.031$ atm) at $T = 300$ K. As regards the dielectric constant, we set $\epsilon = 80$ and $n_1\epsilon'/\epsilon = 1.1$ in accord with Eq.(17).

The other LJ energies in Eq.(77) are given by

$$\epsilon_{1i}/k_B = 287.3, \text{K}, \ \epsilon_{ij}/k_B = 200, \text{K} \ \ (i,j=2,3), \quad (85)$$

which are smaller than ϵ_{11}/k_B and satisfy the Lorentz-Berthelot relations[98] $\epsilon_{ij} = \sqrt{\epsilon_{ii}\epsilon_{jj}}$. For simplicity, we set $\epsilon_{12} = \epsilon_{13}$ not differentiating the properties of cations and anions in water, so we can exchange α_2 and α_3 in our results. In molecular dynamics simulation of aqueous electrolytes[115–117], the pair potentials among ions and water molecules depend on the ion species.

As discussed in Sec.IIIF, to be consistent with the electrostriction data, the Born radii R_i should be smaller than the hardsphere radii $d_i/2$. In this paper, we set

$$R_i = 0.2 d_i \quad (i=2,3). \quad (86)$$

Then, we have $v_i^* < 0$ for $\alpha_i < 0.72$ (see Fig.3(a)). If $R_i = 0.4 d_i$, we have $v_i^* < 0$ for $\alpha_i < 0.58$.

B. Ion volume and interaction coefficients

The solvation coefficient $\nu_i(n_1)$ in Eq.(3) consists of three parts as $\nu_i(n_1) = \nu_i^h - w_{1i} n_1/k_BT + \nu_i^{\rm B}$. Then, from Eq.(19), the ion volume is written as

$$v_i^* = v_i^h + v_i^{\rm LJ} + v_i^{\rm B}. \quad (87)$$

The MCSL part $v_i^h = \epsilon_{\rm in} d\nu_i^h/dn_1$ tends to $v_1\alpha_i^3$ for large α_1 (see Eq.(E4) in Appendix E for its expression). With Eqs.(83)-(86), the LJ part $v_i^{\rm LJ} = -\epsilon_{\rm in} w_{1i}/k_BT$ and the Born part $v_i^{\rm B}$ in Eq.(70) behave as

$$v_i^{\rm LJ}/d_1^3 = -0.11(1+\alpha_i)^3, \quad v_i^{\rm B}/d_1^3 = -0.44/\alpha_i. \quad (88)$$

In Fig.3(a), we examine the three ion-volume parts. For $\alpha_i \lesssim 0.5$, we have $v_i^* \sim v_i^{\rm B} < 0$. For $\alpha_i > 1$, both v_i^h and $v_i^{\rm LJ}$ grow as α_i^3, where $v_i^{\rm B}$ is negligible. In (b), we plot the ratios v_i^*/d_i^3 and $(v_i^h + v_i^{\rm LJ})/d_i^3$ for ϵ_{1i}/k_B =200, 287.5, and 350K, which decrease with increasing ϵ_{1i}. For $\alpha_i \gtrsim 1.2$, we can neglect $v_i^{\rm B}$ and find

$$v_i^* \cong v_1(1+w_{\rm a})\alpha_i^3. \quad (89)$$

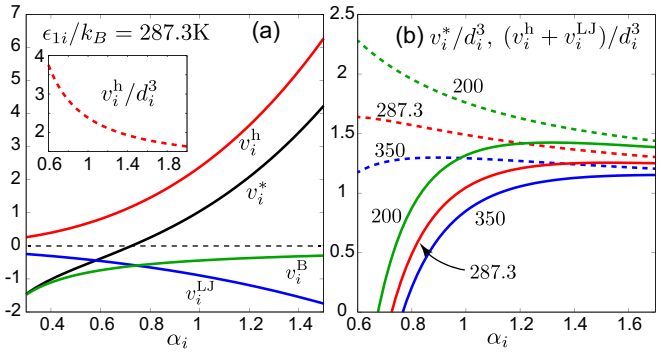


FIG. 3. (Color online) (a) Infinite-dilution ion volume v_i^* (black) composed of v_i^h (red), $v_i^{\rm LJ}$ (blue), and $v_i^{\rm B}$ (green) in units of d_1^3 together with v_i^h/d_i^3 (inset) as functions of $\alpha_i = d_i/d_1$. (b) Ratios v_i^*/d_i^3 (bold line) and $(v_i^h + v_i^{\rm LJ})/d_i^3$ (broken line) for $\epsilon_{1i}/k_B = 200, 287.5$, and 350K. In the other figures, $\epsilon_{1i}/k_B = 287.5$K.

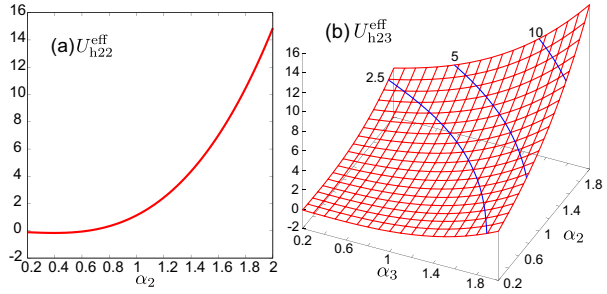


FIG. 4. (Color online) (a) $U_{h22}^{\rm eff}$ vs α_2 and (b) $U_{h23}^{\rm eff}$ in the α_2-α_3 plane in units of $d_1^3 k_B T$, where $\eta_1 = 0.448$ and $\epsilon_{\rm in}^h = 0.028$. These are the effective interaction coefficients in Eq.(92) for purely steric hardsphere mixtures in the MCSL model.

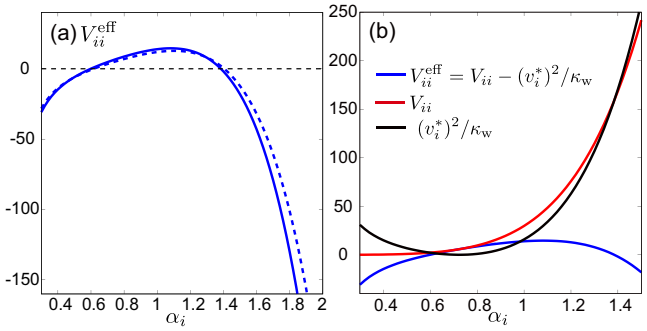


FIG. 5. (Color online) (a) Diagonal (cation-cation or anion-anion) component $V_{ii}^{\rm eff} = V_{ii} - (v_i^*)^2/\kappa_{\rm w}$ in Eq.(91) vs α_i in units of $k_B T d_1^3$. Its approximation in Eq.(99) is also plotted (broken line). (b) Comparison of $V_{ii}^{\rm eff}$ (blue), V_{ii} (red), and $(v_i^*)^2/\kappa_{\rm w}$ (black). For large α_i, the latter two parts grow but mostly cancel, leading to negative $V_{ii}^{\rm eff}$.

See Eq,(E4) and the sentences below it.

To understand the overall behavior of v_i^*, we give a simple interpolation formula,

$$v_i^*/d_1^3 \cong D_{\rm L}\alpha_i^3 - D_{\rm B}/\alpha_i, \tag{90}$$

Here, $D_{\rm L} = \pi(1 + w_{\rm a})/6 = 1.1$ from Eq.(89) and $D_{\rm B} = \epsilon_{\rm in}\ell_B\epsilon'/(0.4d_1^4\epsilon) = 0.44$ from Eqs.(70) and (86). If $v_i^* = 0$, Eq.(90) yields $\alpha_i = 0.80$, while our full equations give $\alpha_i = 0.72$ in Fig.3(a). Previously, some authors[11,12,91–93] wrote the ion volume ($= v_i^* + k_B T\kappa_{\rm w}$) in the form $A_{\rm I}(2r)^3 - B_{\rm I}/r$, where r is a certain ion radius with $A_{\rm I}$ and $B_{\rm I}$ being constants. They set $A_{\rm I} \cong 1.0$ in agreement with our $D_{\rm L} = 1.1$ (if their r is assumed to be close to the crystal radius).

We next show the salient features of the interaction coefficients. From Eq.(5) U_{ij} in Eq.(3) and $U_{ij}^{\rm eff}$ in Eq.(24) include $u_{ij}^{\rm ex}$ in Eq.(6). We calculate the excess parts,

$$\begin{aligned} &V_{ij} = U_{ij} - u_{ij}^{\rm ex}, \quad V_{ij}^{\rm eff} = U_{ij}^{\rm eff} - u_{ij}^{\rm ex}, \\ &V_{\rm eff} = U_{\rm eff} - \frac{1}{2}\sum_{i,j} u_{ij}^{\rm ex}. \end{aligned} \tag{91}$$

We have introduced $\tilde{V}_{\rm eff}$ in Eq.(67). From Eq.(73) V_{ij} consist of the MCSL and LJ parts as $V_{ij} = U_{ij}^h - w_{ij}$.

We consider the purely steric hardsphere parts of $U_{ij}^{\rm eff}$:

$$U_{hij}^{\rm eff} = U_{ij}^h - k_B T n_1 \epsilon_{\rm in}^h (d\nu_i^h/dn_1)(d\nu_j^h/dn_1), \tag{92}$$

which will be explicitly calculated in Appendix E. In Fig. 4, we display $U_{h22}^{\rm eff}/d_1^3 k_B T$ and $U_{h23}^{\rm eff}/d_1^3 k_B T$. The former depends on α_2 only, being nearly zero for $\alpha_2 < 1$ and about 15 for $\alpha_2 \sim 2$. The latter is nearly zero for $\alpha_2 < 1$ and $\alpha_3 < 1$ and are about 10 for $\alpha_2 \sim \alpha_3 \sim 1.8$. The two terms in Eq.(92) are both of order $1200 d_1^3 k_B T$ for $\alpha_2 \sim \alpha_3 \sim 1.8$, so they largely cancel. Thus, $U_{hij}^{\rm eff}$ are smaller than the other contributions with significant attractive and hydration interactions.

Neglecting $U_{hij}^{\rm eff}$ in $V_{ij}^{\rm eff}$, we find some simple limiting behaviors. If α_2 and α_3 are both large, we obtain

$$V_{ij}^{\rm eff}/k_B T v_1 \cong -\alpha_i^3 \alpha_j^3 (w_{\rm a} + w_{\rm a}^2)/\epsilon_{\rm in}, \tag{93}$$

which are largely negative since $\epsilon_{\rm in} \ll 1$. Thus, salts with large-large ion pairs are hardly soluble in water. This is related to the hydrophobic assembly in water, which has been discussed for uncharged large particles[99]. Furthermore, if α_2 is small and α_3 is large, we obtain

$$V_{23}^{\rm eff}/k_B T v_1 \cong -v_2^* \alpha_3^3 (1 + w_{\rm a}) n_1/\epsilon_{\rm in}, \tag{94}$$

which is largely positive for $v_2^* < 0$. Such asymmetric salts are considerably soluble in water[69].

The cancellation of the two hrdsphere parts in Eqs.(24) and (92) is a general feature. It is already indicated by the $\gamma_\pm$-data of $NaBPh_4$[73] (see Sec.IIIE). For a neutral solute, Cerdeiriña and Widom[50] calculated the two terms in Eq.(1) with a smaller difference (see their Fig.3).

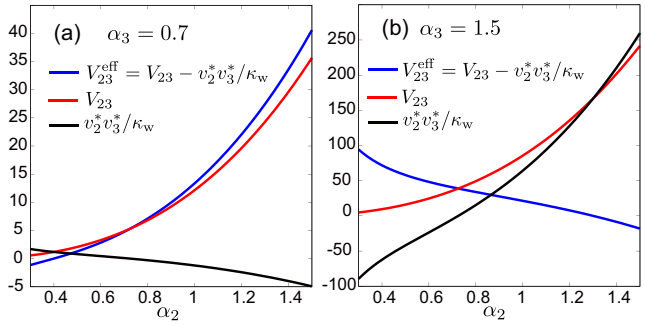


FIG. 6. (Color online) Off-diagonal (cation-anion) components $V_{23}^{\rm eff}$ (blue), V_{23} (red), and $v_2^* v_3^*/\kappa_{\rm w}$ (black) in units of $k_B T d_1^3$ as functions of α_2, where α_3 is (a) 0.7 and (b) 1.5. Here, $v_2^* v_3^*/\kappa_{\rm w}$ is relatively small in (a), while it is largely negative for $\alpha_2 < 0.6$ and largely positive for $\alpha_2 > 1.2$ in (b).

C. Numerical results of $V_{ij}^{\rm eff}$

We present some numerical results. In Fig.5(a), the diagonal component $V_{ii}^{\rm eff}$ in Eq.(91) is plotted vs α_i, which is independent of α_j ($j \neq i$). It is positive in the range $0.60 < \alpha_i < 1.38$ and is negative outside it decreasing as $-$const.α_i^6 for $\alpha_i > 1.5$. We also plot its approximation to be presented in Eq.(98). In (b), we plot $V_{ii}^{\rm eff}$, V_{ii}, and $(v_i)^2/\kappa_{\rm w}$ vs α_i. For $\alpha_i > 1.2$, the latter two are large and close. For $\alpha_i < 0.5$, we have $V_{ii}^{\rm eff} \cong -(v_i^{\rm B})^2/\kappa_{\rm w}$.

In Fig.6, we show the off-diagonal components $V_{23}^{\rm eff}$, V_{23}, and $v_2^* v_3^*/\kappa_{\rm w}$ vs α_2 at fixed α_3. Here, $v_2^* v_3^*/\kappa_{\rm w}$ behaves very differently for (a) $\alpha_3 = 0.7$ and (b) $\alpha_3 = 1.5$ changing its sign at $\alpha_2 = 0.72$. In (a), $V_{23}^{\rm eff}$ and V_{23} are close and monotonically increase with increasing α_2, where $V_{23}^{\rm eff} = 0$ at $\alpha_2 = 0.40$. In (b), $V_{23}^{\rm eff}$ monotonically decreases with increasing α_2 and is negative for $\alpha_2 > 1.30$, where V_{23} and $v_2^* v_3^*/\kappa_{\rm w}$ largely cancel.

In Fig.7, we display $V_{\rm eff}$ and $V_{23}^{\rm eff}$ as functions of α_2 and α_3, whose behaviors change abruptly as α_2 or α_3 changes across 1. (i) They are largely positive for $\alpha_2 < 1 < \alpha_3$ or $\alpha_3 < 1 < \alpha_2$. but are negative if both α_2 and α_3, are large or small. The $V_{\rm eff}$ is mostly close to $\tilde{V}_{\rm eff}$ in Eq.(67). (ii) They increase (decrease) with increasing α_2 for small $\alpha_3 < 1$ (large $\alpha_3 > 1$). See the same tendency in Table II and Fig.2 for alkali hallide salts. (iii) The lines of $\alpha_3 = 1.1$ in (a) and (b) are nearly horizontal in the displayed α_2 range. This explains the marginal behavior of K^+. In Appendix F, we will explain mathematically why $V_{\rm eff}$ and $V_{23}^{\rm eff}$ change their dependence on α_2 at $\alpha_3 \sim 1$.

TABLE III. Example of interaction coefficients V_{ij}, $V_{ij}^{\rm eff}$, and $V_{\rm eff}$ in units of $k_B T d_1^3$ for small-large ion pair.

α_2	α_3	V_{22}	$V_{22}^{\rm eff}$	V_{23}	$V_{23}^{\rm eff}$	V_{33}	$V_{33}^{\rm eff}$	$V_{\rm eff}$
0.7	2	4.86	4.76	78.2	89.6	1108	-291	-53.8

Table III gives V_{ij}, $V_{ij}^{\rm eff}$, and $V_{\rm eff}$ for $(\alpha_2, \alpha_3) = (0.7, 2)$,

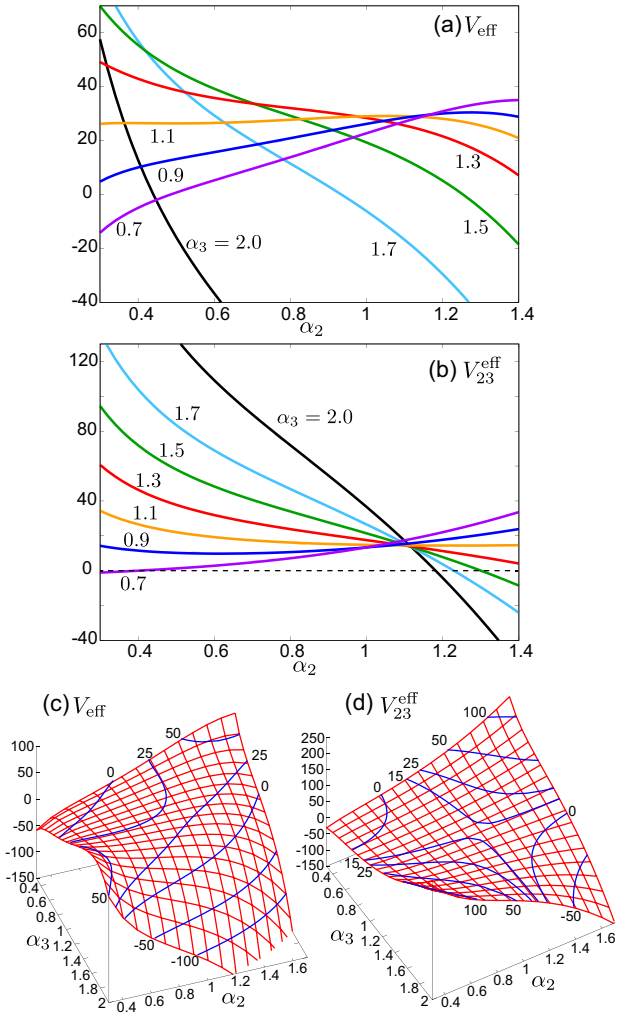


FIG. 7. (Color online) (a) $V_{\rm eff}$ and (b) $V_{23}^{\rm eff}$ in units of $k_B T d_1^3$ vs α_2 for $\alpha_3 = 0.7$, 0.9, 1.1, 1.3, 1.5, and 2.0. Displayed also are bird-eye views of (c) $V_{\rm eff}$ and (d) $V_{23}^{\rm eff}$ in the region $0.35 < \alpha_2 < 1.7$ and $0.35 < \alpha_3 < 2$. They are negative for small-small and large-large pairs, but are positive for small-large pairs (see two peaks)[69]. In (a), the curves decrease into negative regions rapidly for $\alpha_3 > 1.5$ due to diagonal $V_{ii}^{\rm eff}$. The lines of $\alpha_3 = 1.1$ in (a) and (b) are nearly horizontal in the displayed range, which correspond to the contour lines of height 25 in (c) and height 15 in (d).

where $v_2^*/d_1^3 = -0.080$, and $v_3^*/d_1^3 = 9.83$. In this case, V_{33} and $(v_3^*)^2/\kappa_{\rm w}$ are very large and close, leading to $V_{23}^{\rm eff} \sim 90$ and $V_{\rm eff} \sim -50$ in units of $k_B T d_1^3$. For $NaBPh_4$, we expect similar behavior (see Sec.IIIE).

D. Role of hydration for small-large pairs

As in Eq.(94), the interplay of the steric and hydration effects leads to the unique behavior of small-large ion pairs. In $V_{\rm eff}$ in Eq.(91), it give rise to

$$V_{\rm eff}^{\rm B} = |v_{\rm B}|(2v_{\rm s}^* + |v_{\rm B}|)/2\kappa_{\rm w} \tag{95}$$

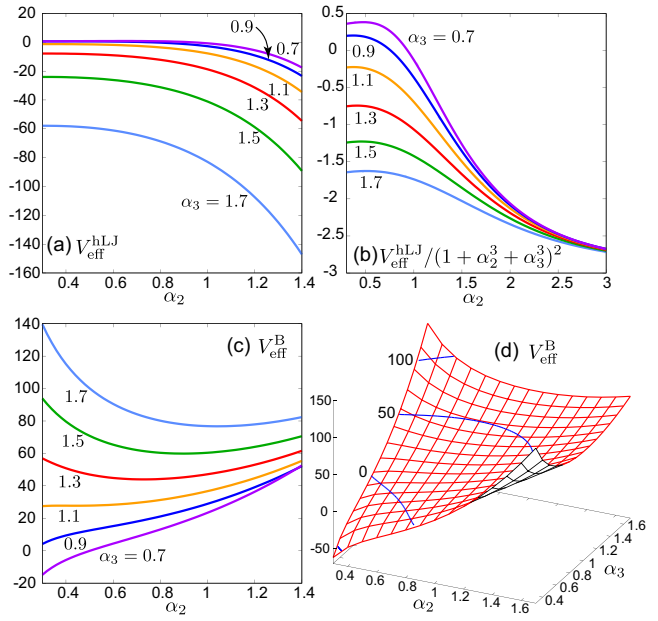


FIG. 8. (Color online) (a) Non-Born coefficient $V_{\rm eff}^{\rm hLJ}$ in Eq.(96), (b) $V_{\rm eff}^{\rm hLJ}/(1+\gamma^2)$ with $\gamma=\alpha_2^3+\alpha_3^3$, and (c) Born coefficient $V_{\rm eff}^{\rm B}$ in Eq.(95) as functions of α_2 for $\alpha_3=0.7, 0.9, 1.1, 1.3, 1.5$, and 1.7. Shown in (d) is $V_{\rm eff}^{\rm B}$ in the α_2-α_3 plane. These are in units of $k_BTd_1^3$.

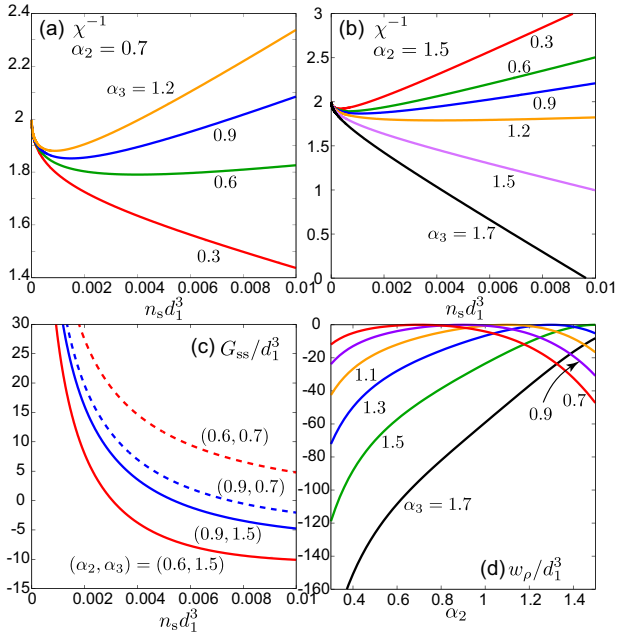


FIG. 9. (Color online) χ^{-1} vs $n_{\rm s}d_1^3$ for $\alpha_3=0.3, 0.6, 0.9$, and 1.2, where α_2 is (a) 0.7 and (b) 1.5 and use is made of Eq.(D1). (c) $w_\rho d_1^3$ in Eq.(33) vs α_2 for $\alpha_3=0.7+0.2m$ $(0\le m\le 5)$, (d) $G_{\rm ss}/d_1^3$ in Eq.(36) vs $n_{\rm s}d_1^3$. for $(\alpha_2,\alpha_3)=(0.6,0.7),(0.9,0.7),(0.9,1.5)$, and $(0.6,1.5)$. Here, the upper bound of the salt density $n_{\rm s}$ is $0.01/d_1^3\sim 0.5$ mol/L.

where $v_{\rm B}=v_2^{\rm B}+v_3^{\rm B}<0$. We then define the non-Born coefficients without hydration as

$$V_{\rm eff}^{\rm hLJ}=V_{\rm eff}-V_{\rm eff}^{\rm B}. \tag{96}$$

In Fig.8, we examine $V_{\rm eff}^{\rm B}$ and $V_{\rm eff}^{\rm hLJ}$. In (a) and (b), $V_{\rm eff}^{\rm hLJ}$ is largely negative for $\gamma=\alpha_2^3+\alpha_3^3>1$ and is small for $\gamma<1$. It is simply approximated by $V_{\rm eff}^{\rm hLJ}/d_1^3k_BT\cong -A\gamma^2/2$ with $A=5.0$. On the other hand, in (c) and (d), $V_{\rm eff}^{\rm B}$ is largely positive for small-large pairs and is negative for small-small pairs.

We can devise a simple approximate expression for $V_{\rm eff}$ in terms of $\gamma=\alpha_2^3+\alpha_3^3$ and $\zeta=1/\alpha_2+1/\alpha_3$ as

$$V_{\rm eff}/d_1^3k_BT\cong B\gamma\zeta-C\zeta^2/2-A\gamma^2/2, \tag{97}$$

where we use Eq.(90). Here, $B=D_{\rm B}D_{\rm L}d_1^3n_1/\epsilon_{\rm in}=7.0$, $C=BD_{\rm B}/D_{\rm L}=2.8$, and $A=5$. In the same manner, we express the cmponents $V_{ii}^{\rm eff}$ and $V_{23}^{\rm eff}$ as

$$V_{ii}^{\rm eff}/d_1^3k_BT\cong 2B\alpha_i^2-C/\alpha_i^2-A\alpha_i^6, \tag{98}$$
$$V_{23}^{\rm eff}/d_1^3k_BT\cong [B(\alpha_2^4+\alpha_3^4)-C]/\alpha_2\alpha_3-A\alpha_2^3\alpha_3^3. \tag{99}$$

These simple expressions can well describe the overall behaviors of $V_{ij}^{\rm eff}$ in Figs.5-7.

E. Numerical results of χ^{-1}, w_ρ, $G_{\rm ee}$, $\ln\gamma_\pm$, and φ

In Fig.9, setting (a) $\alpha_2=0.7$ and (b) 1.5, we plot χ^{-1} vs $n_{\rm s}d_1^3(=0.86n_{\rm s}/n_1)$ for various α_3, We use its extended DH form (D1) with $a_2=a_3=3$ Å, where $n_{\rm s}\chi$ represents the ionic fluctuation variances in Eq.(28). The coefficient of its linear term $2V_{\rm eff}/k_BT$ is negative for small-small ion pairs in (a) and large-large ion pairs in (b). For $(\alpha_2,\alpha_3)=(1.7,1.5)$ in (b), χ^{-1} even decreases to 0, resulting in the instability discussed around Eq.(68). In (c), we also plot the ion-ion KB integral $G_{\rm ss}$ in Eq.(36) vs $n_{\rm s}$ for four sets of (α_2,α_3). It grows as $n_{\rm s}^{-1/2}$ as $n_{\rm s}\to 0$.

In Fig.9(d), we show w_ρ in Eq.(33) vs α_2 for various α_3, which is nonpositive, vanishing for $\alpha_2=\alpha_3$. From Eqs.(98) and (99), we obtain its approximation,

$$\frac{w_\rho}{d_1^3}=-B(\alpha_2-\alpha_3)^2\Big[\frac{\alpha_2}{\alpha_3}+\frac{\alpha_3}{\alpha_2}+1+\frac{C/2B}{(\alpha_2\alpha_3)^2}+\frac{A}{2B}\Big]. \tag{100}$$

Here, we use Eq.(85). For general ϵ_{ij}, Eq.(33) gives $w_\rho=(2w_{23}-w_{22}-w_{33})/2k_BT$ at $\alpha_2=\alpha_3$ in the MCSL model. In particular, w_ρ is largely negative for large-small ion pairs with $\alpha_2<1<\alpha_3$, for which $w_\rho/d_1^3\cong -7\alpha_3^3/\alpha_2$.

In Fig.10, we plot $\ln\gamma_\pm$ and vs $n_{\rm s}d_1^3$ for various α_2 and α_3. We use the extended DH expressions (64)-(66) with $a_2=a_3=3$ Å. These curves are above (below) DH limiting ones if $\tilde{U}_{\rm eff}$ in Eq.(57) is positive (negative) from Eqs.(56) and (62). In (a) and (c), $\tilde{U}_{\rm eff}=-5.0k_BTd_1^3$ for $(\alpha_2,\alpha_3)=(0.7,2)$. Many authors displayed $\ln\gamma_\pm$ and φ for salts with positive linear coefficients[1,2,15,16].

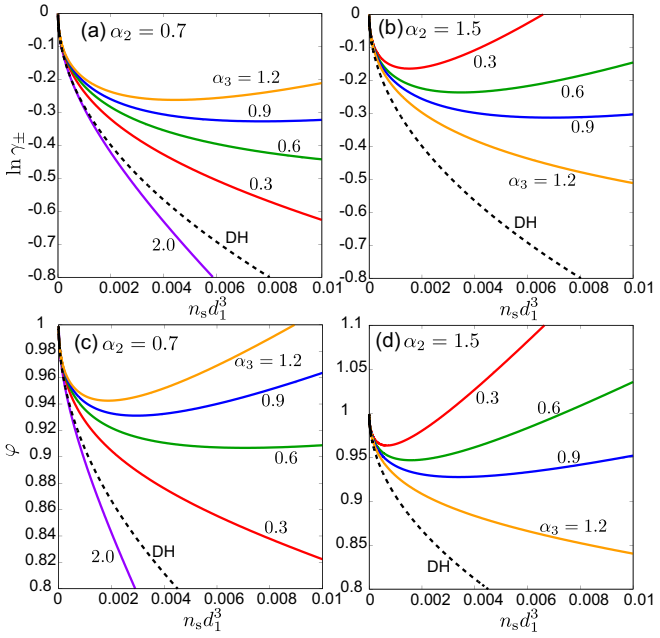


FIG. 10. (Color online) $\ln\gamma_\pm$ and φ in Eqs.(64)-(66) as functions of $n_s d_1^3$ for $\alpha_3 = 0.3, 0.6, 0.9$, and 1.2, where α_2 is 0.7 in (a) and (c) and is 1.5 in (b) and (d). The DH limiting curves are also shown (broken lines).

F. Deviation constant h

Finally, we examine the deviation constant h in the apparent partial volume v_s^{ap} in Eq.(59)[11,22,23,74]. Experimentally, the ion-size-dependence of h is opposite to that of $\ln\gamma_\pm$ and φ, as shown in Table IV. (i) We first consider alkali halides[23]. For F^-, h decreases as the cation size increases. For the other anions, it exhibits the reverse dependence on the cation size. On the other hand, for cations of not large size (Li^+, Na^+, and K^+), h decreases as the anion size increases. For large Rb^+ and Cs^+, h behaves non-monotonically. (ii) Second, for tetraalkylammonium Et_4N^+ halides[22], h is negative and increases with increasing the anion size.

In our scheme, the unique behavior of h arises if $\partial\tilde{V}_{\rm eff}/\partial p$ exceeds $\kappa_w\tilde{V}_{\rm eff}$ in Eq.(60). In particular, v_i^B depends on n_1, so we consider the ratio $A_B = n_1(\partial v_i^B/\partial n_1)/v_i^B$. From Eq.(70) it is expressed as

$$A_B = (\partial^2\epsilon/\partial p^2)/(\epsilon\kappa_w^2 a_\epsilon) - 2a_\epsilon, \qquad (101)$$

where $a_\epsilon = n_1\epsilon'/\epsilon = 1.1$ in Eq.(17) and R_i is assumed to be independent of n_1. Here, data of ϵ in ambient water[89,90] give $(\partial^2\epsilon/\partial p^2)_T \sim -6\times10^{-7}/\mathrm{MPa}^2$. Thus, we estimate $A_B \sim -5$.

In Fig.11, we plot h and $\partial\tilde{U}_{\rm eff}/\partial p$ vs α_2 for various α_3 setting $A_B = -7.5$, where $\partial\tilde{U}_{\rm eff}/\partial p$ determines the overall behavior of h. The resultant h behaves in the same manner as in the the experiment[23]. Here, the two terms in Eq.(60) compete delicately depending on the parameter values. Indeed, if we set $A_B = -5.0$ with the other parameters unchanged, the curves of $\alpha_3 = 0.7, 0.9$, and 1.1 increase with increasing α_2 for $\alpha_2 \gtrsim 0.8$. We also set $n_1\partial\ln\kappa_w/\partial n_1 = -8.3$, from Eqs.(80) and (81), though it is -5.4 in real water[129]. Thus, to calculate h, we need to make very crude approximations[21].

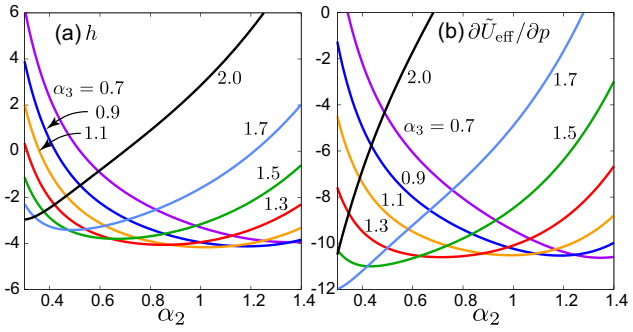


FIG. 11. (Color online) (a) Deviation constant h in Eq.(60) and (b) $\partial\tilde{U}_{\rm eff}/\partial p$ (the second term in Eq.(60)) vs α_2 in units of d_1^6, where $\alpha_3 = 0.7, 0.9, 1.1, 1.3, 1.5, 1.7$, and 2.0 from above.

TABLE IV. Data of h for alkali halides[23] and Et_4N^+ halides[22] in units of $\mathrm{cm}^3\mathrm{L/mol}^2$ and in units of d_1^6 in the parentheses (). Here, 1 $\mathrm{cm}^3\mathrm{L/mol}^2$ corresponds to $3.82d_1^6$ with $d_1 = 3$Å. Ion volume of Et_4N^+ is $v_2^* \sim 9d_1^3 \sim 8n_w^{-1}$.

	F^-	Cl^-	Br^-	I^-
Li^+	1.1 (4.2)	-0.36 (-1.4)	-0.60 (-2.3)	
Na^+	0.64 (2.4)	-0.03 (-0.11)	-0.26 (-0.99)	-0.38 (-1.5)
K^+	0.52 (2.0)	0.10 (0.38)	-0.16 (-0.61)	-0.39 (-1.5)
Rb^+	0.55 (2.1)	0.17 (0.65)	-0.26 (-0.99)	-0.05 (-0.19)
Cs^+	0.25 (0.95)	0.12 (0.46)	0.09 (0.34)	0.11 (0.42)
Et_4N^+		-21.0 (-80)	-19.4 (-74)	-6.0 (23)

V. SUMMARY AND REMARKS

In summary, we have presented a theory of electrolytes accounting for the deviation of the solvent density δn_1 induced by those of the ions. It has been neglected in the previous primitive theories. In Sec.III, we have then derived the ion volume v_i^* in Eq.(19) and the effective ion-ion interaction coefficients $U_{ij}^{\rm eff}$ in Eq.(24) ($i, j = 2, 3$). In the latter, the second bilinear term $(-v_i^* v_j^*/\kappa_w)$ arises from the solvent-mediated interactions and can explain Collins' rule[69] in the presence of the electrostriction (which leads to $v_i^* < 0$ for small ions). Namely, it yields cation-anion repulsion for small-large ion pairs with $v_i^* v_j^* < 0$ and attraction for symmetric pairs with $v_i^* v_j^* > 0$. In the thermodynamic quantities, the mean interaction coefficient $U_{\rm eff} = \sum_{i,j=2,3} U_{ij}^{\rm eff}/2$ appears.

We have defined a parameter χ in the ionic fluctuation variances for n_2 and n_3 in Eq.(28) and expressed the

Kirkwood-Buff integrals for n_1 and n_2+n_3 in terms of χ in Eqs.(36) and (37). We have expanded this χ, the mean activity coefficient $\gamma_\pm$, the osmotic coefficient φ, and the apparent partial volume $v_i^{\rm ap}$ in powers of $\sqrt{n_{\rm s}}$ for small average salt density $n_{\rm s}=\langle n_2\rangle=\langle n_3\rangle$. In these expressions the first correction are the DH contributions.

We have also confirmed unique behavior of small-large ion pairs as predicted by Collins, where $U_{\rm eff}<0$ and $U_{23}^{\rm eff}>0$. As an extreme example, $NaBPh_4$ is strongly coupled with the water density with a largely negative $U_{\rm eff}$. For such a salt, we have discussed a spinodal instability for $n_{\rm s}$ exceeding $n_{\rm s}^{\rm spi}$ in Eq.(68)[67].

In Sec.IV, we have performed numerical analysis using the Mansoori-Carnahan-Starling-Leland (MCSL) model[61], the Lennard-Jones (LJ) attraction, and the Born model. We have calculated the ion volume v_i^* and the excess coefficients $V_{ij}^{\rm eff}=U_{ij}^{\rm eff}-u_{ij}^{\rm ex}$ in Eq.(91) in Fig.7, where $u_{ij}^{\rm ex}$ are the contribution from the DH free energy in Eq.(6). Some asymptotic expressions have been given for them in Eqs.(90), (93), and (94). Regarding the ion-specific thermodynamic behavior, the mean interaction coefficient $U_{\rm eff}=\sum_{i,j=2,3}U_{ij}^{\rm eff}/2$ is a key quantity (see Eqs.(56)-(62))

We have found that the two steric parts in $U_{ij}^{\rm eff}$ in Eq.(24) or $V_{ij}^{\rm eff}$ in Eq.(91) mostly cancel, as calculated in Appendix E. Due to this cancellation, the effective interaction coefficients for purely steric hardsphere systems, $U_{hij}^{\rm eff}$ in Eq.(92), are not large as in Fig.4 and become smaller than the other contributions for ambient water, leading to Eqs.(93) and (94). Note that our hardcore quantities, ν_i^h and U_{ij}^h in Eq.(74) and $1/\epsilon_{\rm in}^h$ in Eq.(81), are enlarged by the powers of $(1-\eta_1)^{-1}$ for large solvent volume fraction $\eta_1(\sim 0.5$ for ambient water). In contrast, in the primitive models[24–28], the total packing fraction arises from the ions only and $U(=-k_BT\sum_{i,j}\int d\boldsymbol{r}c_{ij}^0(r)/2)$ is positive and not very large (see Eq.(22)), so its expression (without the second term in Eq.(25)) was fitted to data of salts.

We have examined the Born part in $V_{ij}^{\rm eff}$, which yields singular interaction for small-large ion pairs. The remaining part consists of the MCSL and LJ contributions exhibiting rather simple behaviors in Fig.8. We have then presented simple interpolation formulas for $V_{ij}^{\rm eff}$ in Eqs.(97)-(99). We have calculated χ^{-1}, w_ρ, $\ln\gamma_\pm$, and φ as functions of α_2, α_3, and $n_{\rm s}$ in Figs.9 and 10. We have also examined the deviation constant h in $v_{\rm s}^{\rm ap}$ in Fig.11, which behaves differently from the others.

We make some remarks.
(i) Our numerical analysis is very approximate. In particular, the parameter choices in Eqs.(83)-(86) remain still arbitrary, where the specific properties of cations and anions are neglected. Nevertheless, our theory provides simple, overall understanding of the puzzling behaviors of electrolytes. The results in Fig.7 should be commonly expected for various solvents (see Appendix F). (ii) We should calculate the structure factors of water and ions at finite wave numbers including the DH interaction and the effective mutual interactions. (iii) It is informative to perform molecular dynamics simulations for various ion pairs, for example, to confirm the behaviors in Fig.7 and Eqs.(97)-(99). (iv) We have mentioned singular behaviors of small-large ion pairs in water[69], which include antagonistic salts[76] such as $NaBPh_4$. It is of great interest to perform scattering experiments[70] for salts with small or negative χ^{-1}. (v) In mixture solvents such as water-alcohol, the solvent-mediated interaction is much enhanced due to the concentration fluctuations[67]. Thus, we need to study electrolytes of mixture solvents.

ACKNOWLEDGMENTS

RO would like to thank Tomonari Sumi for informative discussions. RO acknowledges support from JSPS KAKENHI Grant (No. JP18K03562 and JP18KK0151). KK acknowledges support from JSPS KAKENHI Grant (No. JP18KK0151 and JP20H02696). AO would like to thank Zhen-Gang Wang for informative correspondence.

AIP Publishing Data Sharing Policy
The data that support the findings of this study are available from the corresponding author upon reasonable request.

Appendix A: Bjerrum dipoles

Here, we examine how the Bjerrum dipoles alter our theory. For nonvanishing dipole density $n_{\rm d}$, we change the free energy density f in Eq.(2) to[85]

$$\tilde{f}=f+k_BTn_{\rm d}[\ln(n_{\rm d}\lambda_{\rm d}^3)-1-\nu_{\rm d}+2\nu], \tag{A1}$$

where $k_BT\nu_{\rm d}$ is the free energy decrease due to the association per dipole and ν is defined by Eq.(8). If we neglect inhomogeneous density deviations, we have $n_2=n_3=n_{\rm s}-n_{\rm d}$, where $n_{\rm s}$ is the added salt density (held fixed here). In equilibrium, the dipole chemical potential $\mu_{\rm d}=\partial\tilde{f}/\partial n_{\rm d}$ equals $\mu_{\rm s}$ in Eq.(41); then,

$$n_{\rm d}=Kn_{\rm s}^2+\cdots, \quad n_2=n_3=n_{\rm s}-Kn_{\rm s}^2+\cdots. \tag{A2}$$

where $n_{\rm s}\ll K^{-1}$ with K being the association constant,

$$K=(\lambda^6/\lambda_{\rm d}^3)\exp(\nu_{\rm d}). \tag{A3}$$

If $n_{\rm d}$ is removed, the free energy density is lowered as

$$\tilde{f}(n_1,n_2,n_3,n_{\rm d})=f(n_{\rm w},n_{\rm s},n_{\rm s})-k_BTKn_{\rm s}^2+\cdots, \tag{A4}$$

where the logarithmic term $k_BTn_{\rm d}\ln(n_{\rm d}\lambda_{\rm d}^3)$ disappears. Thus, if we accept Bjerrum's assumption, U_{23} in Eq.(3) is changed to $U_{23}-k_BTK$. Then, $\ln\gamma_\pm$ decreases by $Kn_{\rm s}$.

Appendix B: Gibbs free energy of electrolytes

We calculate the Gibbs free energy G. As in Sec.IIID, we fix p, T, and the total solvent number $N_{\rm w}=Vn_{\rm w}=$

$V_0 n_{\rm w}^0$. Here, without salt at pressure p, the solvent density is $n_{\rm w}^0$ and the volume is V_0.

We integrate $dG/dN_{\rm s} = \mu_{\rm s}$ with respect to $N_{\rm s}$ using Eq.(41), where we set $n_{\rm s} = N_{\rm s}/V \cong (N_{\rm s}/V_0)(1 - \bar{v}_{\rm s}^0 N_{\rm s}/V_0)$ in $\ln(n_{\rm s}\lambda^3)$. Up to order $n_{\rm s}^2$, we obtain[1,18]

$$G = N_{\rm w}\mu_{\rm w}^0(n_{\rm w}^0) + 2k_BTN_{\rm s}[\ln(\lambda^3 N_{\rm s}/V_0) - 1 + \nu(n_{\rm w}^0)] + V_0(-k_BT\kappa^3/12 + \tilde{U}_{\rm eff} n_{\rm s}^2), \quad \text{(B1)}$$

where $\mu_{\rm w}^0(n_{\rm w}^0)$ is the chemical potential of pure solvent at the density $n_{\rm w}^0$ and $\tilde{U}_{\rm eff}$ is given in Eq.(57).

Since $n_{\rm w}^0$ is determined by p and T, we can treat G in Eq.(B1) as a function of $N_{\rm w}$, $N_{\rm s}$, p, and T. Then,

$$V = (\partial G/\partial p)_{N_{\rm w},N_{\rm s},T} = V_0 + v_{\rm s}^{\rm ap} N_{\rm s}, \quad \text{(B2)}$$

from which we can calculate the apparent partial volume $v_{\rm s}^{\rm ap}$ to derive Eqs.(59) and (60) up order $n_{\rm s}^2$. The partial volume $\bar{v}_{\rm s}$ in Eq.(46) can be related to $v_{\rm s}^{\rm ap}$ as

$$\bar{v}_{\rm s} = [v_{\rm s}^p + n_{\rm s}(\partial v_{\rm s}^p/\partial n_{\rm s})]/[1 + n_{\rm s}^2(\partial v_{\rm s}^p/\partial n_{\rm s})], \quad \text{(B3)}$$

where $\partial v_{\rm s}^p/\partial n_{\rm s}$ is the derivative at fixed p and T. On the other hand, from $G = N_{\rm w}\mu_{\rm w} + N_{\rm s}\mu_{\rm s}$, the osmotic coefficient φ in Eq.(61) is expressed as

$$\varphi = [N_{\rm w}\mu_{\rm w}^0(n_{\rm w}^0) + N_{\rm s}\mu_{\rm s} - G]/(2k_BTN_{\rm s}), \quad \text{(B4)}$$

leading to Eq.(62) with the aid of Eqs.(41) and (B1).

Appendix C:Derivation of Eqs.(50) and (59)

We rewrite Eqs.(49) and (58) as

$$dn_{\rm w}/dn_{\rm s} = b_1(n_{\rm w}) + b_2(n_{\rm w})n_{\rm s}^{1/2} + b_3(n_{\rm w})n_{\rm s} + \cdots, \quad \text{(C1)}$$

where b_1, b_2, and b_3 are functions of $n_{\rm w}$. Up to order $n_{\rm s}^2$, Eq.(C1) yields the deviation $\delta n_{\rm w} = n_{\rm w}(n_{\rm s}) - n_{\rm w}^0$ as

$$\delta n_{\rm w} = b_1(n_{\rm w})n_{\rm s} + \frac{2}{3}b_2(n_{\rm w})n_{\rm s}^{3/2} + \frac{1}{2}c_3(n_{\rm w})n_{\rm s}^2 + \cdots = b_1(n_{\rm w}^0)n_{\rm s} + \frac{2}{3}b_2(n_{\rm w}^0)n_{\rm s}^{3/2} + \frac{1}{2}\tilde{c}_3(n_{\rm w}^0)n_{\rm s}^2 + \cdots, \quad \text{(C2)}$$

where the second line is written in terms of $n_{\rm w}^0$ as in Eqs.(50) and (59). Thus, $b_1(n_{\rm w}) \cong b_1(n_{\rm w}^0) + b_1'\delta n_{\rm w}$, where $b_1' = db_1/dn_{\rm w}$. We differentiate the first line of Eq.(C2) with respect to $n_{\rm s}$ to find

$$c_3 = b_3 - b_1 b_1', \quad \tilde{c}_3 = b_3 + b_1 b_1'. \quad \text{(C3)}$$

The expression for $\tilde{c}_3$ leads to Eqs.(50) and (59).

Appendix D: Extended expressions of χ^{-1} and $v_{\rm s}^{\rm ap}$

We rewrite χ^{-1} in Eq.(32) and $v_{\rm s}^{\rm ap}$ in Eq.(59) as

$$\chi^{-1} = 2 - \frac{1}{4}\ell_B\kappa \sum_{i=2,3} \frac{1}{(1+a_i\kappa)^2} + \frac{2n_{\rm s}}{k_BT}V_{\rm eff}, \quad \text{(D1)}$$

$$v_{\rm s}^{\rm ap} = \bar{v}_{\rm s}^0(n_{\rm w}^0) + \epsilon_{\rm in}\ell_B\kappa \sum_{i=2,3}\Big[\frac{\epsilon'/2\epsilon}{1+a_i\kappa} - \frac{\sigma(a_i\kappa)}{6n_{\rm w}}\Big] + [\kappa_{\rm w}\tilde{V}_{\rm eff} + \partial\tilde{V}_{\rm eff}/\partial p]n_{\rm s}. \quad \text{(D2)}$$

We define $V_{\rm eff}$ in Eq.(91) and $\tilde{V}_{\rm eff}$ in Eq.(57). In Eq.(D2), the first term is $\bar{v}_{\rm s}^0$ at the initial density $n_{\rm w}^0$ and $\sigma(x)$ is defined below Eq.(65). These expressions tend to Eqs.(32) and (59) as $a_i\kappa \to 0$.

Appendix E: MCSL model of hardsphere fluids

Here, we summarize the MCSL model of hardsphere fluid mixtures of m components[61], where $m = 3$ in this paper. Setting $n = \sum_i n_i$, $\eta_i = \pi n_i d_i^3/6$, $\eta = \sum_j \eta_j$, and $u = \eta/(1-\eta)$, we write $f_h(n_1, n_2, n_3)$ in Eq.(73) as[130,63]

$$\frac{f_h}{k_BTn} = 4u + u^2 - 3y_1u + (y_3 - 1)[u + u^2 + \ln(1-\eta)]. \quad \text{(E1)}$$

Setting $\sigma_\ell = \sum_i \pi d_i^\ell n_i/6$, we define y_1 and y_3 as

$$y_1 = 1 - 6\sigma_1\sigma_2/(\pi n\eta), \quad y_3 = 6\sigma_2^3/(\pi\eta^2 n), \quad \text{(E2)}$$

where $y_1 \to 0$ and $y_3 \to 1$ in the one-component limit.

From Eq.(E1) we obtain the MCSL chemical potentials $\partial f_h/\partial n_i$. In the dilute case, ν_i^h in Eq.(74) are written as

$$\nu_i^{\rm h} = (3\alpha_i + 6\alpha_i^2 - \alpha_i^3)u_1 + (3\alpha_i^2 + 4\alpha_i^3)u_1^2 + 2\alpha_i^3 u_1^3 + (3\alpha_i^2 - 2\alpha_i^3 - 1)\ln(1-\eta_1), \quad \text{(E3)}$$

where $u_1 = \eta_1/(1-\eta_1)$. The right hand side steeply grows with increasing η_1 (see Fig.3 in our previous paper[66]). The MCSL ion volume $v_i^h = \epsilon_{\rm in} d\nu_i^h/dn_1$ is given by

$$v_i^h = (w_{\rm a} + 1 - \epsilon_{\rm in}u_1^2)\alpha_i^3 v_1 + \epsilon_{\rm in}\psi_i v_1, \quad \text{(E4)}$$

where $v_1 = \pi d_1^3/6$ and $w_{\rm a}$ is defined in Eq.(82). Setting $x_1 = 1/(1-\eta_1)$, we define ψ_i by

$$\psi_i = 6\alpha_i^2 x_1^3 + 3\alpha_i x_1^2 + (1 - 3\alpha_i^2)x_1. \quad \text{(E5)}$$

For $\alpha_i = 1$, we simply find $v_i^h = n_1^{-1}(1 + w_{\rm a} - \epsilon_{\rm in})$. For considerably large α_i (say, $\alpha_i \sim 1.4$), the second term in Eq.(E4) is of order v_1, but it is considerably cancelled by negative $v_i^{\rm LJ}$ (see Fig.3). We thus find Eq.(89).

From Eqs.(E1) and (74) we express U_{ij}^h as

$$U_{ij}^h/v_1k_BT = \alpha_i^3\alpha_j^3\Phi_1 + \alpha_{ij}^2(\alpha_{ij} + 3\alpha_i\alpha_j u_1)/(1-\eta_1) + 6\alpha_i^2\alpha_j^2\Big[(\alpha_{ij}-1)\Big(u_1^3 + 2u_1^2 + \zeta_1\Big) + u_1/(1-\eta_1)^2\Big], \quad \text{(E6)}$$

where $\alpha_{ij} = \alpha_i + \alpha_j$ and $\zeta_1 = -1 - \eta_1^{-1}\ln(1-\eta_1)$. Using ψ_i we also express $U_{hij}^{\rm eff}$ in Eq.(92) as

$$U_{hij}^{\rm eff}/v_1k_BT = \alpha_i^3\alpha_j^3\Phi_2 + 3\alpha_i^2\alpha_j^2(\alpha_{ij}-1)(2\zeta_1 - u_1) + 3\alpha_i^2\alpha_j^2(3-\eta_1)u_1/(1-\eta_1) + \alpha_{ij}^3 + 3\alpha_{ij}\alpha_i\alpha_j u_1 + \epsilon_{\rm in}^h\eta_1[(\psi_i\alpha_j^3 + \psi_j\alpha_i^3)u_1^2 - \psi_i\psi_j]. \quad \text{(E7)}$$

As the coefficients of $\alpha_i^3\alpha_j^3$, we define Φ_1 and Φ_2 as

$$\Phi_1 = \Phi_2 + \eta_1(1 - u_1^2\epsilon_{\rm in}^h)^2/\epsilon_{\rm in}^h, \quad \text{(E8)}$$

$$\Phi_2 = 2\eta_1/(1-\eta_1) + \eta_1 - 6\zeta_1 - \epsilon_{\rm in}^h\eta_1 u_1^4, \quad \text{(E9)}$$

where Φ is large ($\gg 1$) but Φ_2 is small ($\ll 1$) for $\eta_1 \sim 0.5$. In fact, $\Phi_2 \cong \eta_1^3/2$ for $\eta_1 \ll 1$ and $\Phi_2 \sim 0.1$ for

$\eta_1 \sim 0.5$. Thus, the first term in Eq.(E7) is negligible for not very large $\alpha_i\alpha_j$. For small α_i and α_j ($\ll 1$), we have $U_{hij}^{\rm eff}/v_1 k_B T \cong -\epsilon_{\rm in}\eta_1/(1-\eta_1)^2$. We plot $U_{hij}^{\rm eff}$ in Fig.4.

Now, we rewrite $V_{ij}^{\rm eff}$ in Eq.(91) as

$$V_{ij}^{\rm eff} = U_{hij}^{\rm eff} - w_{ij} - (v_i^* v_j^* - v_i^h v_j^h \epsilon_{\rm in}^h/\epsilon_{\rm in})/\kappa_{\rm w}, \quad \text{(E10)}$$

where the MCSL contribution is subtracted in the third term. Here, the third term dominates over the first with significant attractive and hydration interactions. The above expression leads to Eqs.(93) and (94).

Appendix F: Marginal ion-size-dependence

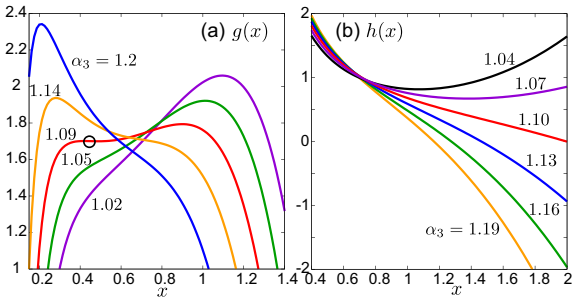


FIG. 12. (Color online) (a) $g(x) = V_{\rm eff}/(k_B T d_1^3 B\alpha_3^2)$ in Eq.(F1) vs $x = \alpha_2/\alpha_3$ at fixed α_3. Line of $\alpha_3 = 1.09$ has an inflection point (○). (b) $h(x) = V_{23}^{\rm eff}/(k_B T d_1^3 B\alpha_3^2)$ in Eq.(F6). These functions are nearly flat for $\alpha_3 \cong 1.1$.

We first show the existence of an inflection point in $V_{\rm eff}$ vs α_2, where $\partial V_{\rm eff}/\partial\alpha_2 = \partial^2 V_{\rm eff}/\partial\alpha_2^2 = 0$ at a certain α_3. Using Eq.(97), we define $g(x) = V_{\rm eff}/(k_B T d_1^3 B\alpha_3^2)$. As a function of $x = \alpha_2/\alpha_3$ at fixed α_3, $g(x)$ is expressed as

$$g(x) = (1+\frac{1}{x})\Big[(1+x^3) - \frac{C'}{2}(1+\frac{1}{x})\Big] - \frac{A'}{2}(1+x^3)^2, \quad \text{(F1)}$$

where $C' = C/B\alpha_3^4 = D_{\rm B}/(D_{\rm L}\alpha_3^4)$ and $A' = A\alpha_3^4/B$ with $A = 5.0$, $B = 7.0$, and $C = 2.8$ (see below Eq.(97)), so we fix $A'C' = 0.29$. We require $dg/dx = d^2g/dx^2 = 0$ at the inflection point to obtain

$$3x^4 - x^3 + x^2 - x + C' = 3A'x^5(x^2 - x + 1), \quad \text{(F2)}$$
$$12x^3 - 3x^2 + 2x - 1 = 3A'x^4(7x^2 - 6x + 5), \quad \text{(F3)}$$

The *critical* values of x and C' are $x_c = 0.45$ and $C_c' = 0.25$, respectively. The critical value of α_3 is given by

$$\alpha_{3c} = (D_{\rm B}/D_{\rm L}C_c')^{1/4} = 1.09. \quad \text{(F4)}$$

which is close to 1 owing to the small exponent 1/4. However, x_c is considerably smaller than 1, so the right hand sides of Eqs.(F2) and (F3) are negligible near the inflection point. For small $\alpha_3 - \alpha_{3c}$ and $x - x_c$, we find

$$g(x) \cong 7(x-x_c)^3 - 16(\alpha_3 - \alpha_{3c})(x - x_c) + 1.7. \quad \text{(F5)}$$

Thus, the slope of $g(x)$ vs x changes its sign abruptly for $\alpha_3 \cong \alpha_{3c}$ as in Fig.7(a), which is analogous to the isothermal pressure-density relation in the van der Waals equation of state.

TABLE V. Values of ϵ, ℓ_B (Å), $(\partial \ln\epsilon/\partial p)_T$ (GPa^{-1}), d_1 (Å), β_1, and α_{3c} for six solvents at $T = 300$ K.

	ϵ	ℓ_B	$\partial\ln\epsilon/\partial p$	d_1	β_1	α_{3c}
water	80	7	0.47	3	0.91	1.09
formamide	111	5	0.45	3.9	0.62	0.74
methanol	33	17	1.2	3.9	1.09	1.31
ethanol	25	22	1.2	4.4	1.03	1.24
acetonitrile	37	15	1.1	4.3	0.96	1.15
acetone	21	27	1.6	4.8	1.07	1.28

Second, we consider the normalized cation-anion interaction coefficient $h(x) = V_{23}^{\rm eff}/(k_B T d_1^3 B\alpha_3^2)$. From Eq.(99), $h(x)$ depends on $x = \alpha_2/\alpha_3$ as

$$h(x) = (1 - A')x^3 + (1 - C')/x, \quad \text{(F6)}$$

which has no inflection point. However, if $A' \cong 1$ or $\alpha_3 \cong (B/A)^{1/4} \sim 1.1$, $h(x)$ is nearly flat, say, in the range $[0.6, 1.2]$ as in Fig. 12(b). For example, we have $A' = 1.05$ and 0.94 for $\alpha_3 = 1.10$ and 1.07, respectively. This behavior can be seen in Fig.7(b).

Third, we discuss the marginal size-dependence of $V_{\rm eff}$ for nonaqueous solvents. From Eq.(F4) and the sentences below Eq.(90), we have $\alpha_{3c} = \beta_1\beta_2$ with

$$\beta_1 = [4\ell_B\epsilon_{\rm in}\epsilon'/\epsilon]^{1/4}/d_1, \quad \beta_2 = (d_i/2R_i D_{\rm L})^{1/4}, \quad \text{(F7)}$$

where we set $C_c' = 1/4$. We also set $\beta_2 = 1.2$ as in the case of water, while β_1 depends on the solvent species. For nonaqueous solvents, we assume $d_1 = n_1^{-1/3}$ and use published experimental data at $T \sim 300$K and $p \sim 1$ atm[94,131]. We then obtain Table V, where $\alpha_{3c} \sim 1$ for all the solvents (again largely due to the exponent 1/4).

[1] R. A. Robinson and R. H. Stokes, *Electrolyte Solutions*, 2nd ed. (Dover: Mineola, NY, 2002).
[2] C. H. Hamann, A. Hamnett, and W. Vielstich, *Electrochemistry* (Wiley-VCH, 2007).
[3] P. Debye and E. Hückel, Phys. Z. **24**, 185 (1923).
[4] D. McQuarrie, *Statistical Mechanics, Chap.15* (Harper and Row, New York, 1976).
[5] W. Kunz, P. L. Nostro, and B. W. Ninham, Curr. Opin.

Coll. Int. Sci. **9**, 1 (2004).
[6] W. Kunz, Curr. Opin. Coll. Int. Sci. **15**, 34 (2010).
[7] P. L. Nostro and B. W. Ninham, Chem. Rev. **112**, 2286 (2012).
[8] W. Kunz, J. Henle, and B. W. Ninham, Curr. Opin. Coll. Int. Sci. **9**, 19 (2004). English translation of Franz Hofmeister's historical papers .
[9] E. Hückel, Z. Phys. **28**, 93 (1925).
[10] M. Born, Z. Physik **1**, 45 (1920).
[11] F. J. Millero, Chem. Rev. **71**, 147 (1971).
[12] Y. Marcus, Chem. Rev. **111**, 2761 (2011).
[13] G. N. Lewis and M. Randall, J. Am. Chem. Soc. **43**, 1112 (1921).
[14] J. N. Brönsted, J. Am. Chem. Soc. **44**, 938 (1922).
[15] E. A. Guggenheim, Phi. Mag. **19**, 588 (1935).
[16] E. A. Guggenheim and J. Turgen, Trans. Faraday Soc. **51**, 747 (1955).
[17] L. A. Bromley, AIChE J. **19**, 313 (1973).
[18] K. S. Pitzer, J. Phys. Chem. **77**, 268 (1973).
[19] B. A. Pailthorpe, D. J. Mitchell, and B. W. Ninham, J. Chem. Soc., Faraday Trans. 2 **80**, 115 (1984).
[20] O. Redlich, J. Phys. Chem. **44**, 619 (1940).
[21] O. Redlich and D. M. Meyer, Chem. Rev. **64**, 221 (1964).
[22] B. E. Conway, R. . E. Verrall, and J. E. Desnyers, Trans. Faraday Soc. **62**, 2738 (1966).
[23] J. E. Desnoyers, M. Arel, G. Perron, and C. Jolicoeur, J. Phys. Chem. **73**, 3346 (1969).
[24] J. C. Rasaiah and H. L. Friedman, J. Chem. Phys. **48**, 2742 (1968).
[25] E. Waisman and J. L. Lebowitz, J. Chem. Phys. **52**, 4307 (1970).
[26] L. Blum, Mol. Phys. **30**, 1529 (1975).
[27] J. P. Simonin, L. Blum, and P. Turq, J. Phys. Chem. **100**, 7704 (1996).
[28] W. Ebeling and M. Grigo, J. Solution Chem. **11**, 151 (1982).
[29] Y. Levin and M. E. Fisher, Physica A **225**, 164 (1996).
[30] G. Stell, J. Stat. Phys. **78**, 197 (1996).
[31] D. N. Card and J. P. Valleau, J. Chem. Phys. **52**, 6232 (1970).
[32] J. M. Romero-Enrique, G. Orkoulas, A. Z. Panagiotopoulos, and M. E. Fisher, Phys. Rev. Lett. **85**, 4558 (2000).
[33] P. S. Ramanathan and H. L. Friedman, J. Chem. Phys. **54**, 1086 (1971).
[34] L. Blum, J. Chem. Phys. **61**, 2129 (1974).
[35] J. Perkyns and B. M. Pettitt, J. Chem. Phys. **97**, 7656 (1992).
[36] Y. V. Kalyuzhnyi, V. Vlachy, and K. A. Dill, Phys. Chem. Chem. Phys. **12**, 6260 (2010).
[37] I. S. Joung, T. Luchko, and D. A. Case, J. Chem. Phys. **138**, 044103 (2013).
[38] S. Weerasinghe and P. E. Smith, J. Chem. Phys. **119**, 11342 (2003).
[39] B. Hess, C. Holm, and N. van der Vegt, J. Chem. Phys. **124**, 164509 (2006).
[40] B. Hess, C. Holm, and N. van der Vegt, Phys. Rev. Lett **96**, 147801 (2006).
[41] I. Kalcher and J. Dzubiella, J. Chem. Phys. **130**, 134507 (2009).
[42] L. Vrbka, M. Lund, I. Kalcher, J. Dzubiella, R. R. Netz, and W. Kunz, J. Chem. Phys. **131**, 154109 (2009).
[43] B. Klasczyk and V. Knecht, J. Chem. Phys. **132**, 024109 (2010).
[44] M. Fyta and R. R. Netz, J. Chem. Phys. **136**, 124103 (2012).
[45] M. Kohns, M. Schappals, M. Horsch, and H. Hasse, J. Chem. Eng. Data **61**, 4068 (2016).
[46] N. Naleem, N. Bentenitis, and P. E. Smith, J. Chem. Phys. **148**, 222828 (2018).
[47] J. G. Kirkwood and F. P. Buff, J. Chem. Phys. **19**, 774 (1951).
[48] B. Widom and R. C. Underwood, J. Phys. Chem. B **116**, 9492 (2012).
[49] K. Koga, V. Holten, and B. Widom, J. Phys. Chem. B **119**, 13391 (2015).
[50] C. A. Cerdeiriña and B. Widom, J. Phys. Chem. B **120**, 13144 (2016).
[51] W. G. McMillan and J. E. Mayer, J. Chem. Phys. **13**, 276 (1945).
[52] R. Evans and T. J. Sluckin, Mol. Phys. **40**, 413 (1980).
[53] A. Onuki, Phys. Rev. E **73**, 021506 (2006).
[54] M. Z. Bazant, M. S. Kilic, B. D. Storey, and A. Ajdari, Adv. Coll. Int. Sci. **152**, 48 (2009).
[55] D. Ben-Yaakov, D. Andelman, R. Podgornik, and D. Harries, Curr. Opin. Colloid Interface Sci. **16**, 542 (2011).
[56] F. Fogolari, A. Brigo, and H. Molinari, J. Mol. Recognit. **15**, 377 (2002).
[57] J. J. Bikerman, Philos. Mag. **33**, 384 (1942).
[58] I. Borukhov, D. Andelman, and H. Orland, Phys. Rev. Lett. **79**, 435 (1997).
[59] V. Kralj-Iglič and A. Iglič, J. de Physique II **6**, 477 (1996).
[60] A. Onuki, *Phase Transition Dynamics* (Cambridge, 2002). In this book, discussions are given on the fluctuation variances in Sec.1.3 and on the steric interaction in polymer solution in Sec.3.5.
[61] G. A. Mansoori, N. F. Carnahan, K. E. Starling, and T. W. Leland, J. Chem. Phys. **54**, 1523 (1971).
[62] P. M. Biesheuvel and M. van Soestbergen, J. Colloid Interface Sci. **316**, 490 (2007).
[63] P. Zhang, N. M. Alsaifi, J. Wu, and Z.-G. Wang, Macromolecules **49**, 9720 (2016).
[64] N. F. Carnahan and K. E. Starling, J. Chem. Phys. **51**, 635 (1969).
[65] R. Okamoto and A. Onuki, Eur. Phys. J. E **38**, 72 (2015).
[66] R. Okamoto and A. Onuki, J. Phys.: Condens. Matter **28**, 244012 (2016).
[67] R. Okamoto and A. Onuki, J. Chem. Phys. **149**, 014501 (2018).
[68] W. Kunz, K. Holmberg, and T. Zemb, Curr. Opin. Colloid Interface Sci. **22**, 99 (2016).
[69] K. D. Collins, Biophys. J. **72**, 65 (1997).
[70] K. D. Collins, G. W. Neilson, and J. E. Enderby, Biophysical Chemistry **128**, 95 (2007).
[71] K. D. Collins, Quarterly Reviews of Biophysics **52**, e11 (2019).
[72] R. Schurhammer and G. Wipff, J. Phys. Chem. A **104**, 11159 (2000).
[73] T. M. Herrington and C. M. Taylor, J. Chem. Soc., Faraday Trans. 1 **78**, 3409 (1982).
[74] F. J. Millero, J. Chem. Eng. Data **15**, 562 (1970).
[75] K. Sadakane, A. Onuki, K. Nishida, S. Koizumi, and H. Seto, Phys. Rev. Lett. **103**, 167803 (2009).
[76] A. Onuki, S. Yabunaka, T. Araki, and R. Okamoto, Curr. Opin. Coll. Int. Sci. **22**, 59 (2016).
[77] S. Yabunaka and A. Onuki, Phys. Rev. Lett. **119**, 118001 (2017).
[78] N. Tasios, S. Samin, R. van Roij, and M. Dijkstra, Phys. Rev. Lett. **119**, 218001 (2017).

[79] N. Bjerrum, Kgl. Dan. Vidensk. Selsk. Mat.-Fys. Medd. **7**, 1 (1926).
[80] D. E. Smith and L. X. Dang, J. Chem. Phys. **100**, 3757 (1994).
[81] L. Degrève and F. L. B. da Silva, J. Chem. Phys. **110**, 3070 (1999).
[82] Y. Marcus and G. Hefter, Chem. Rev. **106**, 4585 (2006).
[83] S. A. Hassan, J. Phys. Chem. B **112**, 10573 (2008).
[84] C. J. Fennell, A. Bizjak, V. Vlachy, and K. A. Dill, J. Phys. Chem. B **113**, 6782 (2009).
[85] J. Zwanikken and R. van Roij, J. Phys.: Condens. Matter **21**, 424102 (2009).
[86] N. F. A. van der Vegt, K. Haldrup, S. Roke, J. Zheng, M. Lund, and H. J. Bakker, Chem. Rev. **116**, 7626 (2016).
[87] R. M. Adar, T. Markovich, and D. Andelman, J. Chem. Phys. **146**, 194904 (2017).
[88] In the original paper[3], a_2 and a_3 can be different, while they have been equated in most subsequent papers.
[89] D. G. Archer and P. Wang, J. Phys. Chem. Ref. Data **19**, 371 (1990).
[90] D. P. Fernández, A. R. H. Goodwin, E. W. Lemmon, J. M. H. L. Sengers, and R. C. Williams, J. Phys. Chem. Ref. Data **26**, 1125 (1997).
[91] L. G. Hepler, J. Phys. Chem. **61**, 1426 (1957).
[92] P. Mukerjee, J. Phys. Chem. **65**, 740 (1960).
[93] J. Padova, J. Chem. Phys. **39**, 1552 (1963).
[94] V. Mazzinia and V. S. J. Craig, Chem. Sci. **8**, 7052 (2017).
[95] J. P. O'Connell and A. E. DeGance, J. Solution Chem. **4**, 763 (1975).
[96] P. Attard, Phys. Rev. E **48**, 3604 (1993).
[97] R. L. de Carvalho and R. Evans, Mol. Phys. **83**, 619 (1994).
[98] J. P. Hansen and I. R. McDonald, *Theory of Simple Liquids* (Academic, 1986).
[99] D. Chandler, Nature **437**, 640 (2005).
[100] M. Lund, B. Jagoda-Cwiklik, C. E. Woodward, R. Vácha, and P. Jungwirth, Phys. Chem. Lett. **1**, 300 (2010).
[101] T. T. Duignan, D. F. Parsons, and B. W. Ninham, Phys. Chem. Chem. Phys. **16**, 22014 (2014).
[102] A. M. Smith, A. A. Lee, and S. Perkin, J. Phys. Chem. Lett. **7**, 2157 (2016).
[103] R. M. Adar, S. A. Safran, H. Diamant, and D. Andelman, Phys. Rev. E **100**, 042615 (2019).
[104] S. W. Coles, C. Park, R. Nikam, M. Kanduč, J. Dzubiella, and B. Rotenberg, J. Phys. Chem. B **124**, 1778 (2020).
[105] P. G. Kusalik and G. N. Patey, J. Chem. Phys. **86**, 5110 (1987).
[106] K. E. Newman, J. Chem. Soc., Faraday Trans. 1 **85**, 485 (1989).
[107] W. Olivares and D. A. Mcquarrie, J. Phys. Chem. **66**, 1508 (1962).
[108] V. McGahay and M. Tomozawa, J. Non-Cryst. Solids **109**, 27 (1989).
[109] F. J. Millero, G. K. Ward, F. K. Lepple, and E. V. Hoff, J. Phys. Chem. **78**, 1636 (1974).
[110] Y. Luo and B. Roux, J. Phys. Chem. Lett. **1**, 183 (2010).
[111] W. J. Hamer and Y.-C. Wu, J. Phys. Chem. Ref. Data **1**, 1047 (1972).
[112] R. D. Shannon, Acta Crystallogr A **32**, 751 (1976).
[113] C. B. Stubblefield and R. O. Bach, J. Chem. Eng. Data **17**, 491 (1972).
[114] H. Glasbrenner and H. Weingärtner, J. Phys. Chem. **93**, 3378 (1989).
[115] I. S. Joung and T. E. Cheatham-III, J. Phys. Chem. B **113**, 13279 (2009).
[116] J. L. Aragones, E. Sanz, and C. Vega, J. Chem. Phys. **136**, 244508 (2012).
[117] T. Yagasaki, M. Matsumoto, and H. Tanaka, J. Chem.Theory and Computation **16**, 2460 (2020).
[118] R. Okamoto and A. Onuki, Phys. Rev. E **82**, 051501 (2010).
[119] A. Onuki and R. Okamoto, Curr. Opin. Coll. Int. Sci. **16**, 525 (2011).
[120] P. Drude and W. Nernst, Z. Phys. Chem. **15**, 79 (1894).
[121] L. D. Landau and E. M. Lifshitz, *Electrodynamics of Continuous Media* (Pergamon, 1984).
[122] The polarization energy of a water molecule around an ion is $\mu_0|E(r)| \sim 3k_BT/r^2$ (r in Å) outside the hydration shell in ambient water, where $\mu_0 = 2.3$ D. The polarization saturates for $r \lesssim \sqrt{3}$ Å.
[123] Y.-Z. Wei, P. Chiang, and S. Sridhar, J. Chem. Phys. **96**, 4569 (1992).
[124] R. Buchner, G. T. Hefter, and P. M. May, J. Phys. Chem. A **103**, 1 (1999).
[125] A. Levy, D. Andelman, and H. Orland, J. Chem. Phys. **139**, 164909 (2013).
[126] J. Vincze, M. Valiskó, and D. Boda, J. Chem. Phys. **133**, 154507 (2010).
[127] V. Talanquer, C. Cunningham, and D. W. Oxtoby, J. Chem. Phys. **114**, 6759 (2001).
[128] N. F. Carnahan and K. E. Starling, AlChE J. **18**, 1184 (1972).
[129] R. A. Fine and F. J. Millero, J. Chem. Phys. **59**, 5529 (1973).
[130] In the original paper[61], another quantity y_2 also appears. In Eq.(E1), it is removed from the relation $y_2 = 1-y_1-y_3$.
[131] Y. Marcus and G. Hefter, J. Sol. Chem. **28**, 575 (1999).